

Stress history controls the spatial pattern of aftershocks: case studies from strike-slip earthquakes

Murat Utkucu¹ · Hatice Durmuş² · Süleyman Nalbant³

Received: 21 January 2016 / Accepted: 21 August 2016 / Published online: 6 September 2016
© Springer-Verlag Berlin Heidelberg 2016

Abstract Earthquake ruptures perturb stress within the surrounding crustal volume and as it is widely accepted now these stress perturbations strongly correlates with the following seismicity. Here we have documented five cases of the mainshock–aftershock sequences generated by the strike-slip faults from different tectonic environments of world in order to demonstrate that the stress changes resulting from large preceding earthquakes decades before effect spatial distribution of the aftershocks of the current mainshocks. The studied mainshock–aftershock sequences are the 15 October 1979 Imperial Valley earthquake ($M_w = 6.4$) in southern California, the 27 November 1979 Khuli-Boniabad ($M_w = 7.1$), the 10 May 1997 Qa’enat ($M_w = 7.2$) and the 31 March 2006 Silakhor ($M_w = 6.1$) earthquakes in Iran and the 13 March 1992 Erzincan earthquake ($M_w = 6.7$) in Turkey. In the literature, we have been able to find only these mainshocks that are mainly characterized by dense and strong aftershock activities along and beyond the one end of their ruptures while rare aftershock occurrences with relatively lower magnitude reported for the other end of their ruptures. It is shown that the stress changes resulted from earlier mainshock(s) that are close in both time and space might be the reason behind the observed aftershock patterns. The

largest aftershocks of the mainshocks studied tend to occur inside the stress-increased lobes that were also stressed by the background earthquakes and not to occur inside the stress-increased lobes that fall into the stress shadow of the background earthquakes. We suggest that the stress shadows of the previous mainshocks may persist in the crust for decades to suppress aftershock distribution of the current mainshocks. Considering active researches about use of the Coulomb stress change maps as a practical tool to forecast spatial distribution of the upcoming aftershocks for earthquake risk mitigation purposes in near-real time, it is further suggested that the background mainshocks along the neighbouring faults should be taken into account in producing the stress change maps for commenting on aftershock occurrences.

Keywords Coulomb stress · Aftershock triggering · Eastern Turkey · Lut block · Imperial Valley · Seismotectonics

Introduction

An earthquake is not an isolated event and changes stress condition in the surrounding volume of crust, causing both stress increase and decrease on neighbouring faults (Stein 1999, 2003; King 2007). This means that static stress perturbation caused by a mainshock can promote or demote stresses along the neighbouring faults and thus triggers or delays following mainshocks and aftershocks along them. Understanding of these stress interactions can be utilized for interpreting location of future mainshocks (King et al. 1994; Stein et al. 1997; Nalbant et al. 2002; McCloskey et al. 2003; Utkucu et al. 2003; Parsons 2004; Doser et al. 2009; Lin et al. 2011).

✉ Murat Utkucu
mutkucu@sakarya.edu.tr

¹ Department of Geophysics, Faculty of Engineering, Sakarya University, Esentepe Campus, 54187 Serdivan, Sakarya, Turkey

² Department of Geological Engineering, Faculty of Engineering, Dumlupınar University, 43100 Kutahya, Turkey

³ School of Environmental Sciences, University of Ulster, Coleraine, UK

Table 1 Focal and source parameters of the mainshocks, whose background and aftershock seismicity are investigated by means of Coulomb stress changes analysis in the study

No.	Earthquake	Time	Lat. (°)	Lon. (°)	Depth (km)	M_w	Strike (°)	Dip (°)	Rake (°)
1	15.10.1979 Imperial Valley ¹	23:16	32.61	−115.32	15	6.4	143	90	180
2	27.11.1979 Khuli-Boniabad ^{2,3}	17:10	34.06	59.76	8	7.1	261	82	8
3	13.03.1992 Erzincan ^{4,5}	17:18	39.71	39.60	27.2	6.8*	125	78	−167
4	10.05.1997 Qa'ena ^{6,7}	07:57	33.83	59.81	10	7.2	338	89	177
5	31.03.2006 Silakhor ⁸	01:17	33.50	48.78	10	6.1	314	54	180

See Fig. 1 for the epicentral distribution of the mainshocks

* Ms

¹ Hartzell and Heaton (1983); ² Walker et al. (2004); ³ Walker et al. (2011); ⁴ Pinar et al. (1994); ⁵ Tan (2004); ⁶ Berberian et al. (1999); ⁷ Sudhaus and Jonsson (2011); ⁸ United States Geological Survey (USGS)

Spatial correlations between mainshock coseismic stress changes and aftershock occurrences have been globally documented over different tectonic environments (Toda and Stein 2003; Steacy et al. 2005; Raju et al. 2008; Lasocki et al. 2009; Sato et al. 2012; Kassarasa et al. 2014). Tiny stress increases can bolster occurrence of aftershocks (or increase seismicity rates) while a few aftershocks occur (or seismicity rate decreases) in the area of stress drops or stress shadows (Stein 2003; Toda et al. 2012).

One of the main concerns following a destructive mainshock is where and how big the upcoming aftershocks would be in the earthquake struck area. Because, a strong aftershock may enhance the destruction made by the mainshock and cause more fear among the people. A recent example was the 23 October 2011 Van earthquake sequence in the eastern Turkey (Utkucu 2013; Utkucu et al. 2013). A strong aftershock with magnitude $M_w = 5.9$ on 9 November 2011 caused considerable damage and loss of life in the city centre of Van, which experienced relatively low damage and loss of life from the mainshock.

In the present study, coseismic Coulomb stress changes associated with five strike-slip mainshocks occurred in Turkey, Iran and California have been studied with their aftershock distributions (Table 1; Fig. 1). These mainshocks are characterized with relatively dense and strong aftershock activity along and beyond the one end of their ruptures while anomalously sparse and lower magnitude aftershock activity along and beyond the other end of their ruptures. Why such a spatial pattern has been observed is the motivation behind the present study. These observed aftershock patterns are investigated not only by means of stress changes in their respective mainshocks but also by means of stress changes in the background large earthquakes occurred in the near vicinity of these mainshock ruptures as well. Because, the maps of stress changes may

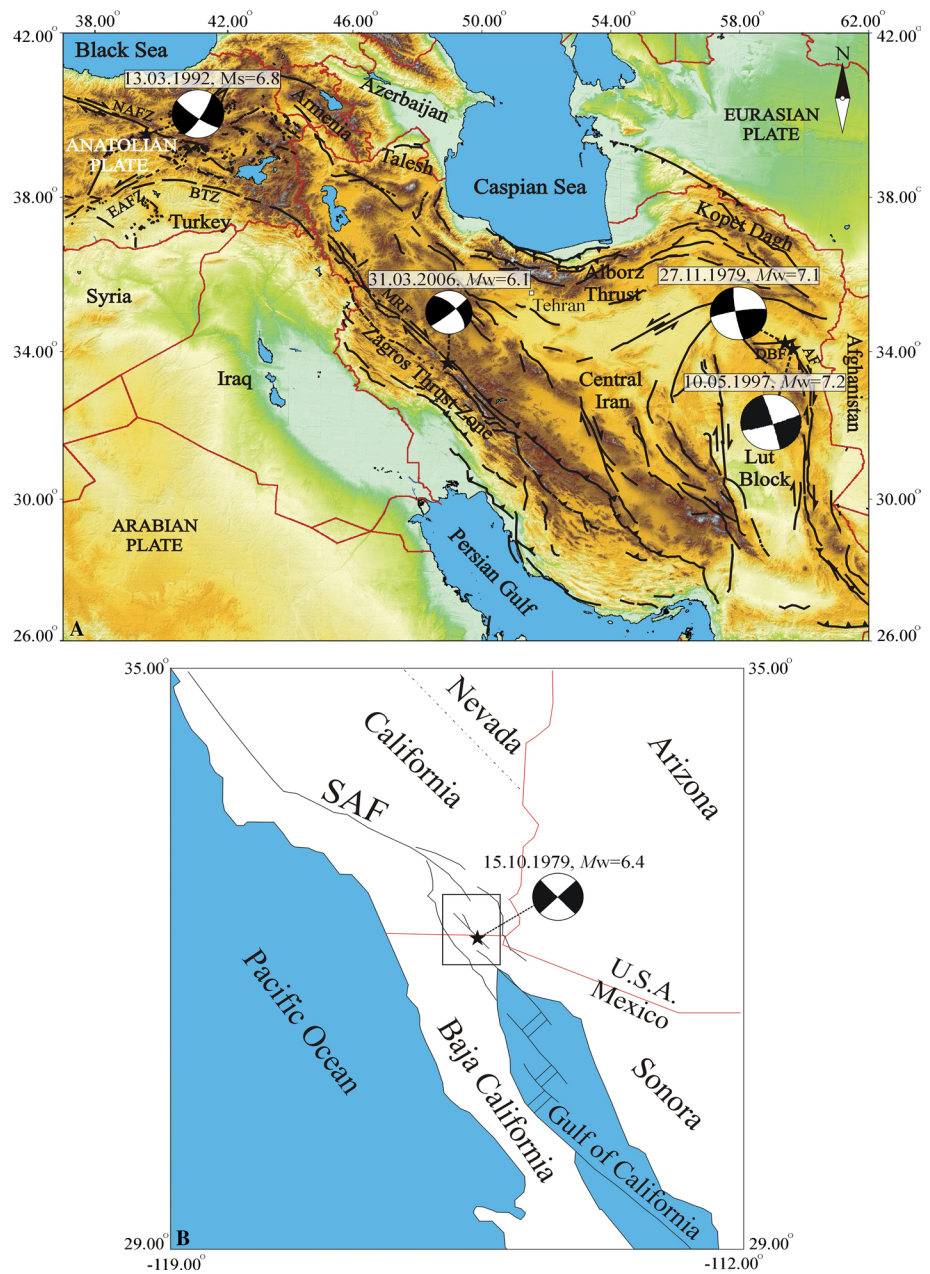
help identification of the areas where aftershocks are much likely to occur and, in turn, may provide a powerful tool for mitigating aftershocks-related earthquake losses (McCloskey and Nalbant 2009).

Tectonic settings of the studied mainshocks

Active tectonics of Turkey and Iran is dominated by the convergence of Arabian and Eurasian plates (Fig. 1a) (Vernant et al. 2004; Copley and Jackson 2006; Reilinger et al. 2006). The Anatolian plate moves to the west along the North and East Anatolian Fault Zones while the boundary of the Arabian and eastern Anatolian block, the Bitlis Thrust Zone, has lesser importance in coping with the convergence-related deformation (McClusky et al. 2000; Sandvol et al. 2003; Reilinger et al. 2006; Bulut et al. 2012). The deformation is mainly accommodated through strike-slip faulting and laterally transported to the Caucasus, Talesh and Alborz thrust zones in eastern Turkey and NW Iran (Jackson 1992; McClusky et al. 2000; Vernant et al. 2004; Djamour et al. 2011).

In contrast to the Bitlis Thrust Zone, the shortening along the Zagros thrust zone is one of the main tectonic elements in accommodating deformation to the farther east (Vernant et al. 2004; Mouthereau et al. 2012). However, comparable amount of deformation is transferred beyond the Zagros Thrust Zone within the Iranian plateau in order to be eliminated along the Alborz and Kopet Dagh mountain ranges through N–S-trending strike-slip faulting and block movement within the Iranian plateau (Vernant et al. 2004; Reilinger et al. 2006). The Main Recent Fault is another major tectonic property in the region and lies parallel to the Zagros Thrust Zone (Talebian and Jackson 2002; Vernant et al. 2004; Reilinger et al. 2006). It accommodates boundary parallel component of the oblique

Fig. 1 Major tectonic elements of **a** eastern Turkey and Iran and **b** southern California. The rectangle in **b** encloses the map areas shown in Figs. 2a and 3. *Black stars and black–white beach balls* represent the epicentres and source mechanisms of the mainshocks studied. Active faults are compiled from MTA (2012), Hessami et al. (2003), Sharp (1982a), and source mechanisms are from Hartzell and Heaton (1983), Pinar et al. (1994), Berberian et al. (1999) and USGS-NEIC. NAFZ North Anatolian Fault Zone, EAFZ East Anatolian Fault Zone, BTZ Bitlis Thrust Zone, MRF Main Recent Fault, DBF Dasht-e Bayaz Fault, AF Abiz Fault, SAF San Andreas Fault



convergence of the Arabian plate along the Zagros Thrust Zone.

The Imperial Valley Region in southern California and NW Mexico is a complicated plate boundary between the North American and Pacific plates and connects the northward progressing spreading ridge complex of the Gulf of California to the San Andreas transform fault system (Fig. 1b) (Allen et al. 1965; Sharp 1982a; Fuis et al. 1982; Rockwell and Klinger 2013). The connection takes place through interlinked fault systems. Although these faults are mainly right-lateral and near-vertical faults striking NW, a number of parallel left-lateral faults that trend NE–SW and appear to connect the right-lateral faults can

also be noticed. The southern part of the San Jacinto fault (the Cayote Creek fault), the Elsinore fault, the Superstition Mountain fault, the Imperial fault, the Laguna Salada fault, the Cerro Prieto fault, the Pescadores fault and the southernmost part of the San Andreas fault are the right-lateral faults lie in the region. The small spreading centres or seismic zones that connect the right-lateral faults represent another conspicuous seismotectonic feature in the region. The Brawley Seismic Zone (BSZ) in the South of the Salton Sea links the San Andreas and Imperial faults and accommodates tectonic deformation between those faults. The BSZ is bounded by Brawley Fault in the east (Meltzner et al. 2006). In the Mexican side of the international border,

the southern end of the Imperial fault is connected with the Cerro Prieto Fault through Cerro Prieto Seismic Zone (CPSZ) or spreading centre. The region is characterized by intense seismic activity with sporadic occurrence of moderate and large magnitude mainshocks (Allen et al. 1965; Johnson and Hill 1982) and earthquake swarms (Johnson and Hadley 1976; Hauksson et al. 2013).

Coulomb stress analysis

The Coulomb failure stress change ($\Delta\sigma_f$) can be simply expressed as:

$$\Delta\sigma_f = \Delta\tau + \mu' \Delta\sigma_n \quad (1)$$

where $\Delta\tau$ and $\Delta\sigma_n$ represent the changes in the shear (positive in the fault slip direction) and the normal stresses (positive for extension) over the target fault plane, respectively, while μ' is the apparent coefficient of the friction (Harris 1998), which includes the unknown effect of pore fluid pressure and has been postulated to vary in the range 0.2–0.8. The selection of value of μ' has been pointed out to be not crucial in affecting the pattern of change in Coulomb failure stress (King et al. 1994; Cocco et al. 2000; Steacy et al. 2004). We have used $\mu' = 0.4$ in our stress calculations and base them on the coseismic elastic dislocation modelling of the earthquakes (Okada 1992) by assuming earthquake ruptures as rectangular dislocation surfaces in an elastic half-space having Young's modulus of 80 GPa and Poisson's ratio of 0.25. Coulomb 3.2 software is used to estimate Coulomb failure stress changes (Lin and Stein 2004; Toda et al. 2005).

Mainshock–Aftershock Sequences Investigated

Following a comprehensive review of the literature, we have been able to obtain only five mainshock–aftershock sequences that have one-sided aftershock distributions and occurred along different strike-slip faults in Turkey, Iran and California for the stress changes analysis. The focal and source parameters of these mainshocks are listed in Table 1, and their epicentre locations are shown in Fig. 1. As we demonstrate below these mainshocks have been followed by more intense and relatively higher magnitude aftershock activity in the one side of their rupture lengths in spite of increases in respective coseismic stresses in the both sides their ruptures as expected (Fig. 2).

The 15 October 1979 Imperial Valley earthquake ($M_w = 6.4$)

The 1979 Imperial Valley earthquake ruptured northern two-third of the Imperial fault, which had been entirely

ruptured by the 19 May 1940 Imperial Valley earthquake ($M_w = 6.9$ – 7.0) (Allen et al. 1965; Sharp 1982b; Sharp et al. 1982; Rockwell and Klinger 2013) (Fig. 2a). Though its surface ruptures were wholly mapped in the south-east California, the epicentre was located in the south of the international border (Chavez et al. 1982) and some relatively minor deep slips for several kilometres southward from the border were obtained through inversion of the seismic waveform data (Hartzell and Heaton 1983). The aftershock activity succeeding the earthquake extended for 100 km in the trend of the mapped surface ruptures and included a $M_L = 5.8$ aftershock a day after the main shock (Fig. 2a) (Johnson and Hutton 1982; Hutton et al. 2010). Though the $M \geq 3.0$ aftershocks higher in number and much stronger (including the largest aftershock of the 16 October 1979 ($M_w = 5.8$)) in the north and NW of the rupture (named as the northern cluster—the NC) (Fig. 2a), the whole 1-year-long activity was characterized by three distinct clusters (inset map in Fig. 2a). The NC was observed over and around the BSZ. A small cluster (the middle cluster—the MC) along the Imperial fault between the epicentre of the mainshock and Brawley fault and another cluster over the CPSZ, well beyond the southern extreme of the surface rupture can be defined (the southern cluster—the SC).

Four large earthquakes occurred in the close vicinity of the 1979 Imperial earthquake since 1930 (Fig. 2a) (Allen et al. 1965; Rockwell and Klinger 2013). The 30 December 1934 Laguna Salada ($M_w = 6.5$) and 31 December 1934 Colorado River ($M_w = 7.0$) earthquakes occurred along the Laguna Salada and Cerro Prieto faults, respectively. The 19 May 1940 Imperial earthquake ($M_w = 7.0$) ruptured whole Imperial fault with displacement as much as 7 m, while the 9 April 1968 Borrego Mountain earthquake ($M_w = 6.5$) was produced by the Cayote Creek fault with 0.4-m peak dislocation. Table 2 lists the source parameters of these background earthquakes.

The 27 November 1979 Khuli-Boniabad earthquake ($M_w = 7.1$)

The 1979 Khuli-Boniabad earthquake ruptured eastern part of the Dasht-e-Bayaz fault that bounds the Lut Block in the North (Figs. 1a, 2b; Table 2) (Berberian and Yeats 1999). Its rupture length was 60 km, along which vertical displacement of as much as 2.5 m and left-lateral displacement of 4 m have been reported (Haghipour and Amadi 1980; Walker et al. 2004, 2011). No other displacement measurement is available. The earthquake was followed an aftershock activity that comprises the 7 December 1979 Kalat-e-Shur earthquake ($M_w = 5.9$) just beyond the eastern tip of the rupture (Berberian et al. 1999; Walker et al. 2011). Epicentral distribution of the available 39 aftershocks with

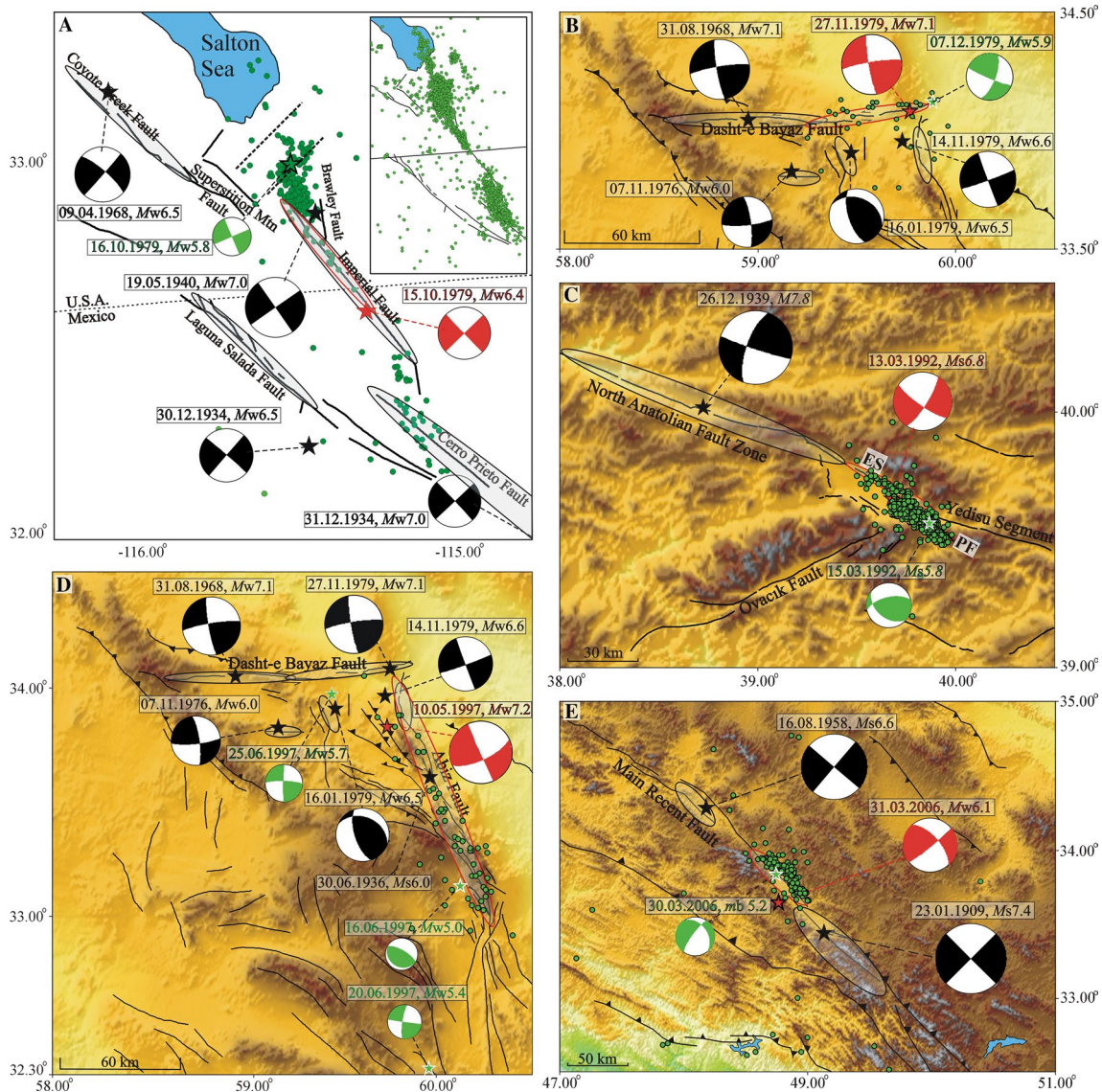


Fig. 2 Local tectonic features, epicentral distributions (black stars), rupture extents (black-outlined elongated ellipses) and source mechanisms (black–white beach balls) of the large background earthquakes in the near source region of the mainshock–aftershock sequences studied. Red stars and red-outlined elongated ellipses denote the mainshocks and the rupture extents of the mainshocks focused in the present study, respectively, while the aftershock locations and source mechanisms are represented with green filled circles (the largest ones with green stars) and green–white beach balls,

$M > 3.5$ aftershocks, 27 of which were relocated by Walker et al. (2011) and 12 of which were taken from International Institute of Earthquake Engineering and Seismology (IIEES) of Iran, is shown in Fig. 2b.

Between the 31 August 1968 Dasht-e-Bayaz and the 1979 Khuli-Boniabad earthquakes, three moderately large earthquakes took place in the near source region (Fig. 2b; Table 2). The first one is the Qayen earthquake of the

respectively. **a** The 15 October 1979 Imperial Valley ($M_w = 6.4$) earthquake mainshock–aftershock sequence with 1-year-long $M \geq 3$ and $M \geq 0.5$ aftershocks (inset map). **b** The 27 November 1979 Khuli-Boniabad ($M_w = 7.1$), **c** the 13 March 1992 Erzincan ($M_w = 6.7$), **d** the 10 May 1997 Qa'enan ($M_w = 7.2$) and **e** the 31 March 2006 Silakhor ($M_w = 6.1$) mainshock–aftershock sequences. See text for the sources from which information presented in the maps compiled. PF Pülümür fault, ES Erzincan segment

7 November 1976 ($M_w = 6.0$), along the EW-trending Avash fault, lying parallel to the Dasht-e-Bayaz fault (Walker et al. 2011). The second one is the 16 January 1979 Boznabad earthquake ($M_w = 6.5$), the source fault of which has not been clearly identified, but NS-trending Boznabad and Pavak faults are possible candidates (Berberian et al. 1999; Walker et al. 2011). The last one is the 14 November 1979 Korizan earthquake ($M_w = 6.6$), which

Table 2 Rupture parameters of the earthquakes selected for the Coulomb stress change analysis of the each mainshock–aftershock sequence studied

Earthquake name	Lat. (°)	Lon. (°)	<i>M_w</i>	Strike (°)		Dip (°)	Rake (°)	Fault length (km)	Fault width (km)	Slip (m)
<i>15.10.1979 Imperial Valley earthquake</i>										
30.12.1934 Laguna Salada	32.25	−115.50	6.5	311 ¹		88 ¹	180 ¹	30	12 ²	0.5 ^a
31.12.1934 Colorado River	32.00	−114.75	7.0	317 ¹		89 ¹	180 ¹	60 ^a	14 ^a	1.5 ^a
19.05.1940 Imperial Valley	32.87	−115.48	7.0	325 ¹		90 ¹	180 ¹	64 ²	12 ^a	Variable ³
09.04.1968 Borrego Mountain	33.19	−116.13	6.5	311 ¹		78 ¹	179 ¹	32 ⁴	10 ^a	Variable ⁴
15.10.1979 Imperial Valley	32.61	−115.32	6.4	143 ⁵		90 ⁵	180 ⁵	40 ⁵	12 ⁵	Variable ⁵
<i>27.11.1979 Khuli-Boniabad earthquake</i>										
31.08.1968 Dasht-e-Bayaz	34.05	58.95	7.1	270		84 ⁶	5 ⁶	75	18.80 ^a	Variable ⁷
07.11.1976 Qayen	33.83	59.17	6.0	84 ⁶		79 ⁶	12 ¹	13.21 ^a	7.07 ^a	0.14 ^a
16.01.1979 Boznabad	33.91	59.47	6.5	162 ⁸		66 ⁸	115 ⁸	28.60 ^a	11.03 ^a	1.00 ^a
14.11.1979 Korizan	33.96	59.73	6.6	S1	190 ⁹	87 ^{6,8}	−177 ^{6,8}	9 ⁸	20	1.00 ^a
				S2	140 ⁹	87 ^{6,8}	−177 ^{6,8}	11 ⁸	20	0.60 ^a
27.11.1979 Khuli-Boniabad	34.06	59.76	7.1	261 ^{6,8}		82 ^{6,8}	8 ^{6,8}	60 ^{6,8}	18.80 ^a	Variable ¹⁰
<i>13.03.1992 Erzincan earthquake</i>										
26.12.1939 Erzincan ¹¹	39.77	39.53	7.8*	S1	114	86	160	20	18	Variable
				S2	106	86	160	51	18	Variable
				S3	112	86	160	31	18	Variable
13.03.1992 Erzincan	39.71	39.60	6.8*	125 ¹¹		78 ¹¹	−167 ¹¹	30 ¹²	18 ¹²	Variable ¹²
<i>10.05.1997 Qa'emat earthquake</i>										
30.06.1936 Abiz	33.61	59.96	6.0*	166 ¹³		87 ¹³	180 ¹³	12 ^{6,12}	6.5 ^a	0.15 ^a
31.08.1968 Dasht-e-Bayaz	34.05	58.95	7.1	270		84 ⁶	5 ⁶	75	18.80 ^a	Variable ⁷
07.11.1976 Qayen	33.83	59.17	6.0	84 ¹		79 ⁶	12 ⁶	13.21 ^a	7.07 ^a	0.14 ^a
16.01.1979 Boznabad	33.91	59.47	6.5	162 ⁸		66 ⁸	115 ⁸	28.60 ^a	11.03 ^a	1.00 ^a
14.11.1979 Korizan	33.96	59.73	6.6	S1	190 ⁹	87 ^{6,8}	−177 ^{6,8}	9 ⁸	20	1.00 ^a
				S2	140 ⁹	87 ^{6,8}	−177 ^{6,8}	11 ⁸	20	0.60 ^a
27.11.1979 Khuli-Boniabad	34.06	59.76	7.1	261 ^{6,8}		82 ^{6,8}	8 ^{6,8}	60 ^{6,8}	18.80 ^a	Variable ¹⁰
10.05.1997 Qa'emat ¹³	33.83	59.81	7.2	S1	190	87	−175	20	20	Variable
				S2	140	87	−175	25	20	Variable
				S3	164	87	−175	30	20	Variable
				S4	330	87	−175	45	20	Variable
				S5	118	87	135	10	20	Variable
<i>31.03.2006 Silakhor earthquake</i>										
23.01.1909 Lurestan ¹⁴	33.41	49.13	7.4*	135		90	180	45	25	2.0
16.08.1958 Firuzabad	34.30	48.17	6.6*	130 ¹⁴		90 ¹⁴	180 ¹⁴	20 ^a	19 ^a	0.5 ^a

Table 2 continued

Earthquake name	Lat. (°)	Lon. (°)	<i>M_w</i>	Strike (°)	Dip (°)	Rake (°)	Fault length (km)	Fault width (km)	Slip (m)
31.03.2006 Silakhor	33.50	48.78	6.1	318	63	174	36 ¹³	16 ¹³	Variable ¹³

S1, S2, S3, S4 and S5 represent segment numbers in the multi-segment rupture parameterization of the earthquakes under interest. See Fig. 2 for the epicentral distribution of the earthquakes used in the study of the each sequence

* *M_s*

^a Wells and Coppersmith (1994)

¹ Freed et al. (2007); ² Deng and Sykes (1997); ³ Rockwell and Klinger (2013); ⁴ Clark (1972); ⁵ Hartzell and Heaton (1983); ⁶ Walker et al. (2011); ⁷ Ambraseys and Tchalenko (1969); ⁸ Walker et al. (2004); ⁹ Berberian et al. (1999); ¹⁰ Haghypour and Amadi (1980); ¹¹ Barka (1996); ¹² Tan (2004); ¹³ Durmuş (2014); ¹⁴ Ambraseys and Melville (1982)

ruptured the northern section of the Abiz fault for 20 km with lateral measured displacement of 1 m (Berberian et al. 1999; Walker et al. 2011). The source parameters of these background earthquakes are given in Table 2.

The 13 March 1992 Erzincan earthquake (*M_w* = 6.7)

The 1992 Erzincan earthquake took place in the eastern section of the notorious North Anatolian Fault Zone (NAFZ), along the Erzincan segment (ES) (Pinar et al. 1994; Barka 1996; Fuenzalida et al. 1997; Grosser et al. 1998; Kaypak 2008) (Figs. 1a, 2c). The ES constitutes northern boundary of the Erzincan basin, which is one of the several pull-apart basin along the NAFZ (Aktar et al. 2004; Kaypak 2008). The 1992 Erzincan earthquake ruptured eastern half of the ES, while the western half had been ruptured by the great Erzincan earthquake of the 26 December 1939 (*M_s* = 7.8–8.0), slip of which tapered down from 5 to 6 m to 1 m along the segment (Barka 1996; Fuenzalida et al. 1997). The earthquake produced no clear surface ruptures but some ground cracks (Fuenzalida et al. 1997). A teleseismic finite-fault modelling of the earthquake indicated a rupture mostly below 5 km for a length of 30 km and slip as much as 1.2 m (Tan 2004). The rupture propagated 20 km to the west and 10 km to the east from the focus. The aftershocks of the earthquake mostly occurred in the SE of the epicentre and include *M_w* = 5.8 shock, namely Pülümür earthquake of the 15 March 1992 (Nalbant et al. 1996; Fuenzalida et al. 1997; Grosser et al. 1998; Kaypak and Eyidoğan 2005; Kalafat et al. 2007) (Fig. 2c). The aftershocks form a cluster that extend from the eastern termination of the ES, where the left-lateral Ovacık fault meets the NAFZ, to Pülümür town in the SE (Fig. 2c). For the time period between 13 March and 30 March 1992, the aftershocks are taken from Kalafat et al. (2007) and are *M* > 3.5. Two weeks after the earthquake, a temporary seismic network was deployed to record the aftershock seismicity and precisely relocated 867 aftershocks with *M* > 1 for the time period 30 March and 22 April 1992 (Kaypak and Eyidoğan 2005). The 1939

Erzincan earthquake is the only large and destructive shock to occur in close vicinity of the 1992 Erzincan earthquake rupture in the instrumental period before 1992.

The 10 May 1997 Qa'emat earthquake (*M_w* = 7.2)

10 May 1997 Qa'emat earthquake occurred along the Abiz fault in the Zirkuh region of Iran near Afghanistan boundary (Figs. 1a, 2d) (Berberian et al. 1999; Gheitanchi and Zarifii 2004; Walker et al. 2011). The Abiz fault extends from Dasht-e-Bayaz fault in the North to the Sepestan Mountain in the South and constitutes NE boundary between the Lut block and the Afghan block. NS-trending strike-slip fault bounding the Lut block accommodates difference in northward crustal motion between eastern and western Iran (Vernant et al. 2004).

The 1997 Qa'emat earthquake produced about 125-km-long multi-segment surface rupture along the Abiz fault (Fig. 2d) (Ikeda et al. 1999; Berberian et al. 1999). Though approximately 1 m of vertical displacement measured along the south-easternmost section of the rupture, the faulting mostly dextral and observed dextral displacements exceed 2 m in some places along the rupture. These observed and complex character of the faulting have been confirmed by both point source (Berberian et al. 1999) and finite-fault (Sudhaus and Jonsson 2011; Durmuş 2014) analysis using teleseismic waveforms and geodetic data.

The 45-day-long aftershock activity of the 1997 Qa'emat earthquake between 10 May and 25 June 1997 comprises 55 aftershocks with magnitude *M* > 3.5 and is compiled from Walker et al. (2011) and USGS-NEIC catalogues (Fig. 2d). Fifty-two of these aftershocks are relocated aftershocks (Walker et al. 2011), while the rest are taken from IIEES of Iran.

The source region of the 1997 Qa'emat earthquake is a seismically active region in the NE Iran where a tectonic system with EW-striking sinistral faults is substituted by the NS-striking dextral fault prevailing tectonic system towards the east (Fig. 2d). Five *M* ≥ 6.0 earthquakes took

place to effect the Abiz fault by means of stress changes in the source region after 1936 (Table 2; Fig. 2d) (Berberian et al. 1999; Berberian and Yeats 1999). These earthquakes are the 30 June 1936 Abiz ($M_s = 6.0$) and the 14 November 1979 Korizan ($M_w = 6.6$) earthquakes that partly ruptured northern half of the Abiz fault, the 31 August 1968 Dasht-e-Bayaz ($M_w = 7.1$) and the 27 November 1979 Khuli-Boniabad ($M_w = 7.1$) earthquakes along the sinistral Dasht-e-Bayaz fault and the 7 November 1976 Qayen ($M_w = 6.0$) and the 16 January 1979 Boznabad ($M_w = 6.5$) earthquakes occurred along the faults within the Lut block. The source parameters of these earthquakes are summarized in Table 2.

The 31 March 2006 Silakhor earthquake ($M_w = 6.1$)

The 2006 Silakhor earthquake took place along the Main Recent Fault, causing 68 lives and about 2000 casualties (Figs. 1a, 2e) (Ramazi and Hosseinnejad 2009; Rezapour 2009; Ghods et al. 2012). Though no surface ruptures were observed following the earthquake, a part of the NW–SE-trending and 100-km-long Dorud fault segment has been assigned as the source fault because of the ground cracks along it and destruction of all of the villages surrounding the fault segment. The earthquake had been preceded by two foreshocks with magnitude $m_b = 4.7$ and 4.9 on 30 March 2006 (not shown here) and an aftershock activity comprising two shocks that having comparable magnitude with the foreshocks (Fig. 2e) (Rezapour 2009; Hamzehloo et al. 2009; Ghods et al. 2012). Source mechanism solutions of the earthquake suggest dextral faulting along a NE dipping fault plane (Rezapour 2009; Hamzehloo et al. 2009; Harvard GCMT; USGS-NEIC). Finite-fault modelling using InSAR (Peyret et al. 2008) and teleseismic (Durmuş 2014) data indicates that slip as much as 0.7–1 m occurred at depth over the rupture plane.

In the near source vicinity, four destructive earthquakes, all of which occurred different fault segments of the Main Recent Faults, preceded the 2006 Silakhor earthquake. These earthquakes are 23 January 1909 Lurestan ($M_s = 7.4$), the 13 December 1957 Farsineh ($M_s = 6.7$), the 16 August 1958 Firuzabad ($M_s = 6.6$) and the 24 March 1963 Karkhaneh ($M_s = 5.8$) earthquakes. However, only the first and the third earthquakes are close enough to alter stress condition of the 2006 Silakhor earthquake rupture plane and are used in the stress changes estimates in the study (Table 2; Fig. 2e).

Modellings and results

In Fig. 3 and in the following figures showing stress change maps as well, the stress changes have been imaged at a

depth of 8 km, which is approximately equal to the half of the seismogenic thickness in the source areas of the earthquakes studied, and shown in map view. Increase and decrease in the stresses are shown as red and blue colours, respectively. Not only the Coulomb failure stresses have been estimated over the optimally oriented strike-slip faults but also over the prescribed rupture planes with the exception of the 1979 Khuli-Boniabad earthquake. The rupture parameters (strike, dip, rake and slip values of the faulting) and respective references for the all earthquakes used in the stress change calculations are given in Table 2. If available, we use variable slip models based on displacement measurements along the surface ruptures and from the inversion of earthquake waveforms and geodetic data. If there is no information to define a variable slip model, slip amplitude of the earthquake is defined regarding the magnitude of the relevant earthquake using the empirical relationships given by Wells and Coppersmith (1994), assuming homogeneous fault slip.

As the aftershock activity of the 1979 Imperial Valley earthquake indicated three distinct clusters over the BSZ and the CPSZ and along the Imperial fault, the stress changes have been mapped over the rupture planes representing these tectonic structures. Figure 3a, b shows the stress changes over the Imperial fault (strike = 143°, dip = 90° and rake = 180°) due to the 1979 Imperial Valley earthquake alone and the four earthquakes in the background together with the 1979 Imperial Valley earthquake, respectively. Next shown in Fig. 3 are the stress changes resolved over the structures-related BSZ and the CPSZ. These structures have been approximated by the NS-trending normal faults (strike = 185°, dip = 50° and rake = -90°) and left-lateral faults (strike = 233°, dip = 66° and rake = -22°) that are conjugate to trend of the Imperial fault (Suarez-Vidal et al. 2008; Hauksson et al. 2013). Stress maps in Fig. 3c, e represent the 1979 Imperial Valley earthquake's stress changes, while Fig. 3d, f shows stress changes in the background earthquakes in addition to the 1979 Imperial Valley earthquake. Figure 3g, h shows the stress changes calculated over the optimally oriented strike-slip faults caused by merely the 1979 Imperial Valley earthquake and including the background earthquakes, respectively. The regional stress directions have been adapted from Heidbach et al. (2008) for the estimation of the stress changes in Fig. 3g, h. With the exception of Fig. 3h in which the lower magnitude threshold is taken as $M \geq 3.0$ aftershocks, in all of the stress maps presented in Fig. 3 comprise 1-year-long $M \geq 0.5$ aftershocks.

Faulting of the background earthquakes in 1934 has been approximated by rupture areas and homogeneous slips after Wells and Coppersmith (1994) (Table 2). Heterogeneous slip distribution has been utilized for both the 1940 Imperial Valley and the 1968 Borrego Mountain earthquakes

Fig. 3 Coulomb failure stress changes resulting from the 15 October 1979 Imperial Valley (maps in the left) and the 1979 Imperial earthquake together with the background earthquakes (maps in the right), which are the 30 December 1934 ($M_w = 6.5$) Laguna Salada, 31 December 1934 Colorado River ($M_w = 7.0$), the 19 May 1940 Imperial Valley ($M_w = 7.0$) and the 9 April 1968 Borrego Mountain ($M_w = 6.5$) earthquakes. The stresses are resolved onto **a, b** the Imperial fault (strike = 143° , dip = 90° and rake = 180°) and **c, d** normal faults (strike = 185° , dip = 50° and rake = -90°) and **e, f** left-lateral faults (strike = 233° , dip = 66° and rake = -22°) inside the Brawley and Cerro Prieto Seismic Zones, **g, h** the optimally oriented strike-slip faults. *Black dots* indicate 1 year-long $M > 0.5$ ($M \geq 3.0$ in **h**) aftershock sequence from Southern California Earthquake Data Centre (Hutton et al. 2010) and active faults traces are from Rockwell and Klinger (2013). *Green star* denotes the epicentre of the 1979 Imperial Valley earthquake. Table 2 summarizes the rupture parameters used in the stress computations. The maps reflect stress changes at depth of 8 km

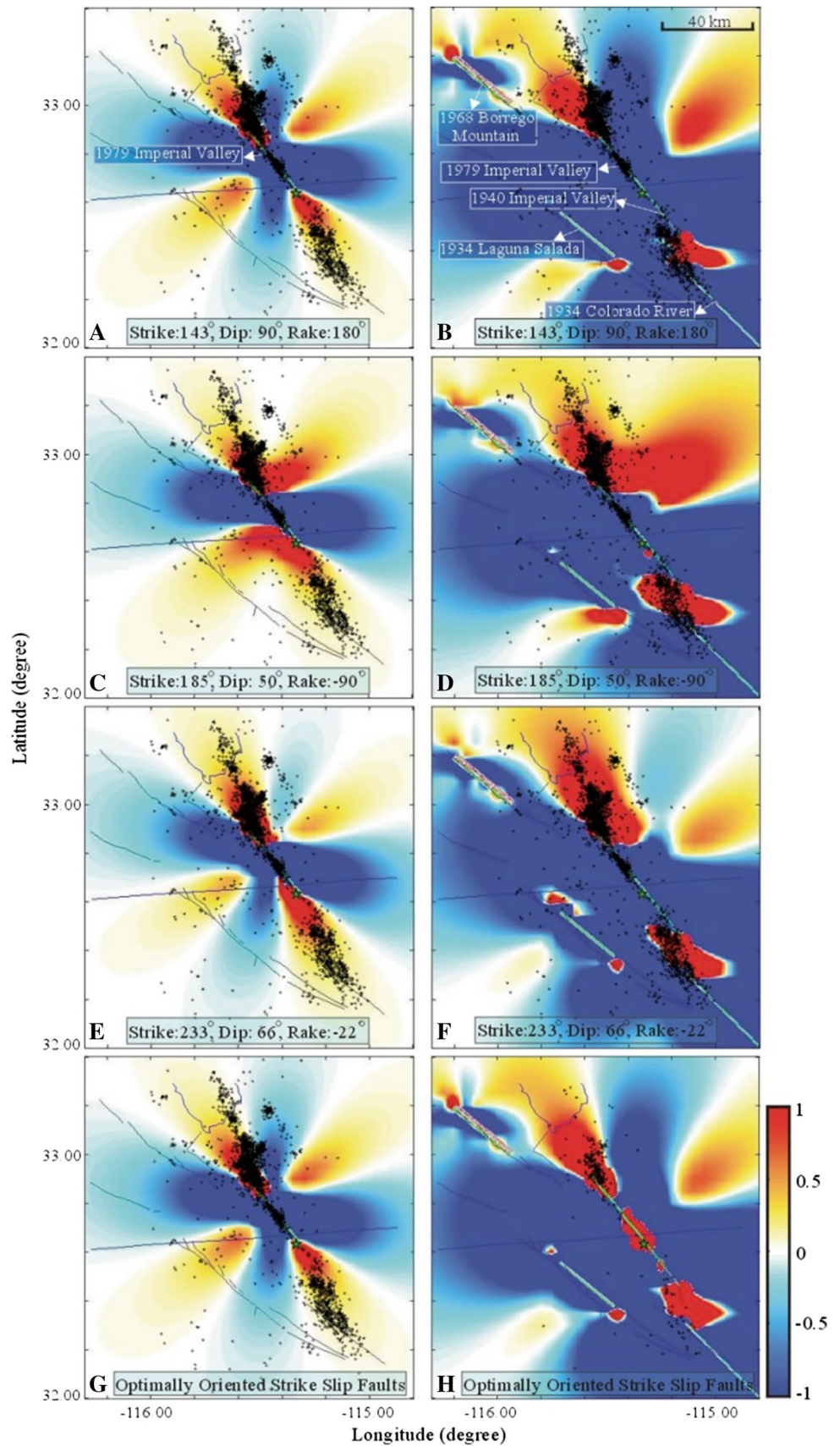
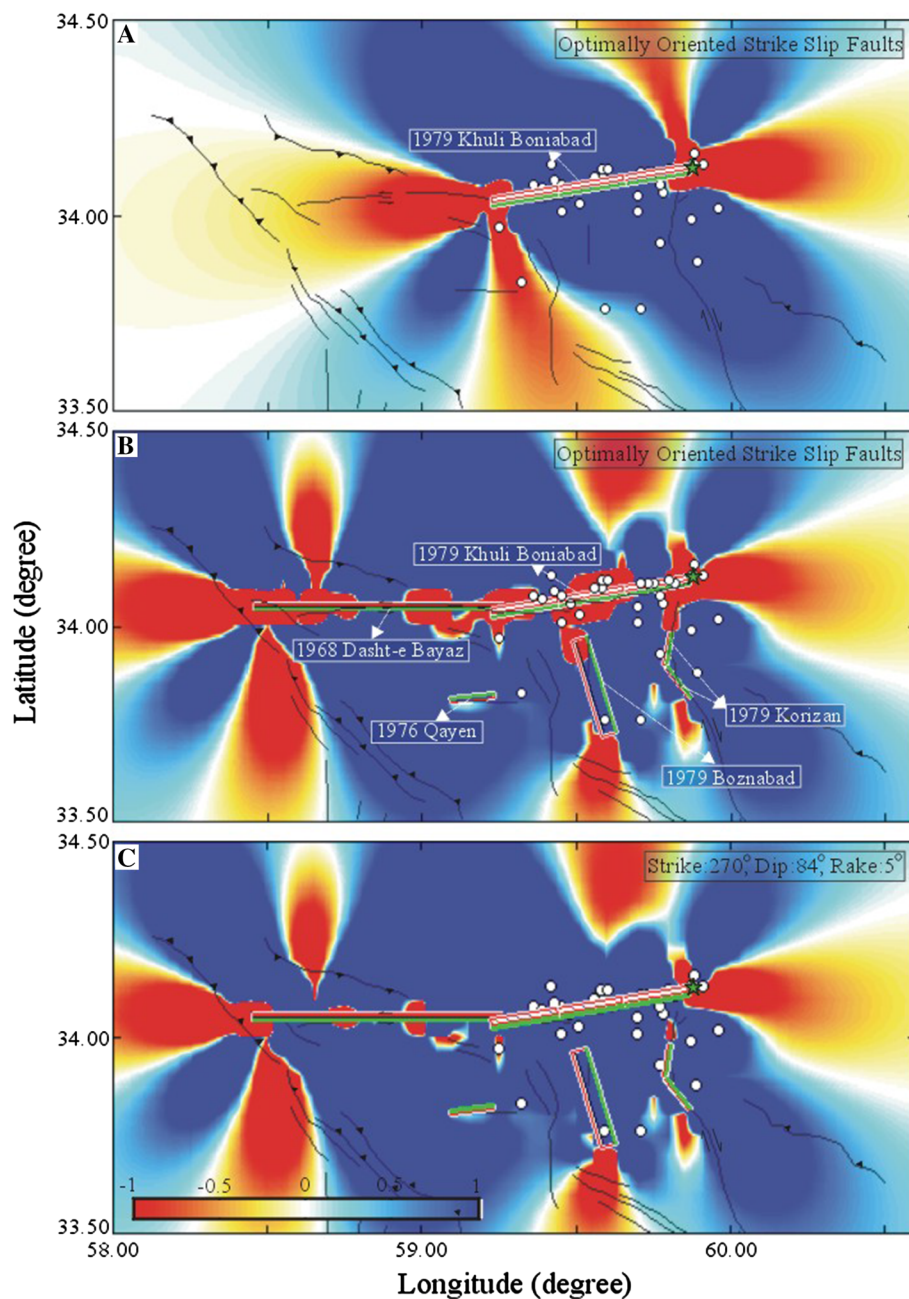


Fig. 4 **a** Coulomb failure stress changes due to the 27 November 1979 Khuli-Boniabad earthquake ($M_w = 7.1$) alone and **b** along with previous mainshocks in the background, resolved onto the optimally oriented strike-slip faults. **c** Coulomb failure stress changes over the 31 August 1968 Dasht-e-Bayaz earthquake rupture plane caused by the 27 November 1979 Khuli-Boniabad and the background earthquakes. The stresses are sampled at depth of 8 km. *White circles* indicates the available $M > 3.5$ aftershocks of the 1979 Khuli-Boniabad earthquake located by Walker et al. (2011) and IIEES of Iran. See Table 2 for the rupture parameters utilized in the stress calculations. Active faults traces are from Berberian et al. (1999)



regarding their observed surface ruptures (Clark 1972; Rockwell and Klinger 2013). For the 1979 Imperial Valley earthquake, finite-fault slip distribution model of Hartzell and Heaton (1983) has been used in the stress changes calculations.

The stress changes due to the 1979 Khuli-Boniabad earthquake alone and the background large earthquakes in addition to the 1979 Khuli-Boniabad earthquake have been computed over the optimally oriented strike-slip faults as shown in Fig. 4a, b along with the available aftershock epicentres. Regional stress directions are taken from Durmuş (2014). Figure 4c is the same as Fig. 4b

for the earthquakes used, but the stress changes have been resolved onto the rupture planes parallel to the 1968 Dasht-e-Bayaz earthquake's rupture plane (strike = 270° , dip = 84° and rake = 5°). Since no variable slip model exists for the earthquake, we used a 60-km-long rupture plane with homogeneous slip of 2 m, which is a product of the empirical relationship of Wells and Coppersmith (1994). However, reverse slip component with 0.3 m slip has been included for the eastern one-third of the rupture plane regarding the slip vector angle (Table 1) and vertical displacement reported by Haghypour and Amadi (1980) for the eastern part of the rupture in the field. Figure 4b shows

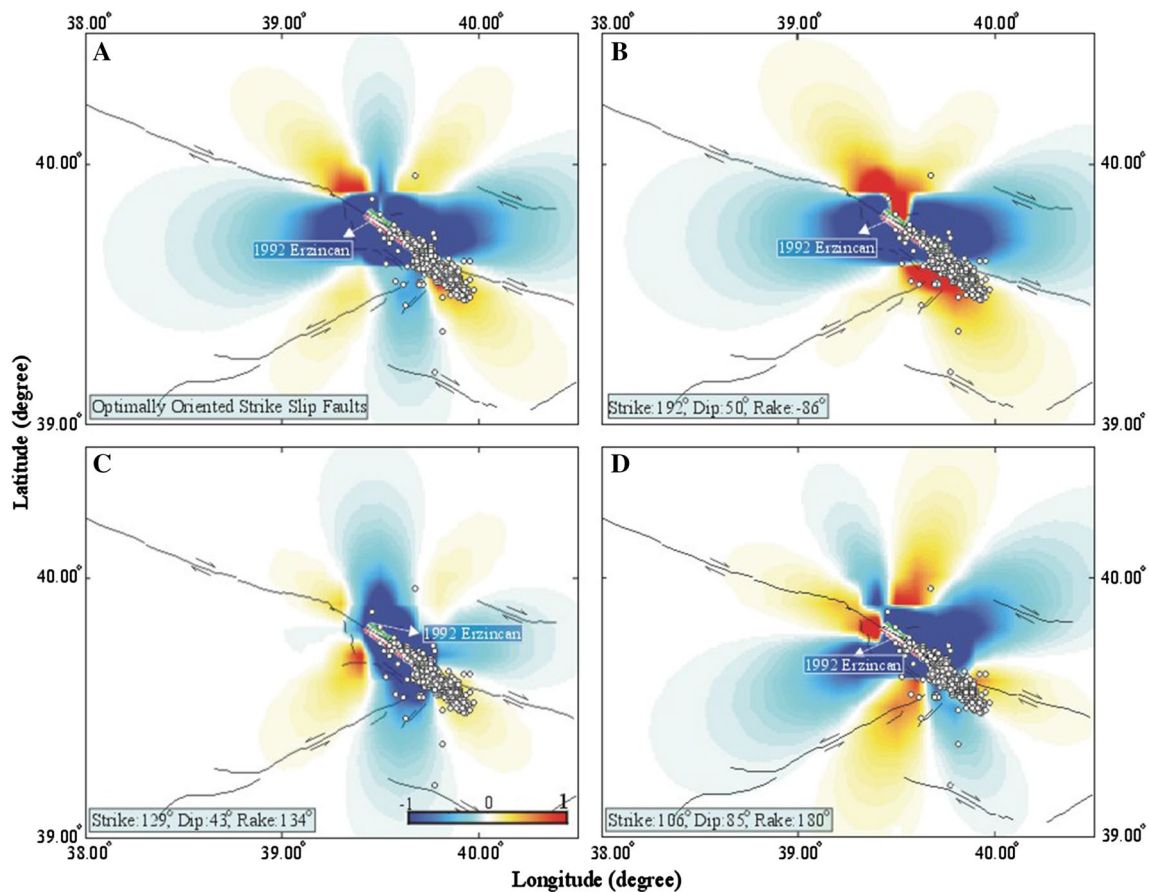


Fig. 5 Coulomb failure stress changes merely due to the 13 March 1992 Erzincan earthquake calculated over **a** the optimally oriented strike-slip faults, **b** the normal faults (strike = 192°, dip = 50° and rake = -86°) bounding the SE edge of the Erzincan basin, **c** the Pülümür fault (strike = 129°, dip = 43° and rake = 134°) and the Yedisu

fault segment (strike = 106°, dip = 85° and rake = 180°). *White circles* indicate the aftershocks compiled from Kaypak and Eyidoğan (2005) and Kalafat et al. (2007). See Table 2 for the rupture parameters. Active faults traces are from MTA (2012). The stress changes are resolved at depth of 8 km

the stress changes in the earthquake along with the previous earthquakes in the background over the optimally oriented strike-slip faults. Ambraseys and Tchalenko (1969) provided both detailed surficial ruptures maps and displacement measurements for the 70 km-long 1968 Dasht-e-Bayaz earthquake rupture. Nevertheless, the surface ruptures along the eastern half of the rupture were discontinuous with slip in the order of tens of centimetres. Therefore, we use a variable slip model for the western part and homogeneous slip with slip amplitudes of 0.7 and 0.1 m for the left-lateral and reverse slip components, respectively. The ruptures of the other three mainshocks have been represented with homogeneous slip regarding empirical relationships given by Wells and Coppersmith (1994).

Figure 5 depicts the Coulomb stress changes produced by the 1992 Erzincan earthquake alone together with the aftershocks. Figure 5a shows the stress condition for the optimally oriented strike-slip faults by using regional stress field with compressional stress axis lying in N–S direction

(Fuenzalida et al. 1997). We also estimate the stress changes along the specified fault planes because fault plane solutions of the aftershocks indicated separate zones of the aftershocks by means of the faulting types. The stress changes are resolved onto the normal faults (strike = 192°, dip = 50° and rake = -86°) along the SE margin of the Erzincan basin (as indicated by the aftershock zones 2 and 3 defined by Fuenzalida et al. (1997)), the Pülümür fault (strike = 129°, dip = 43° and rake = 134°) and along the Yedisu fault segment (strike = 106°, dip = 85° and rake = 180°), which is going to be discussed as a possible source of the largest aftershock, in Fig. 5b–d, respectively. The stress changes from both the 1939 and 1992 Erzincan earthquakes are shown in Fig. 6. The 1939 Erzincan earthquake is the mere large earthquake in the instrumental period to alter stresses in the crust volume surrounding the 1992 Erzincan earthquake. A variable slip model based on the field study of Barka (1996) has been used for the 1939 Erzincan earthquake. Figure 6a represents stress changes

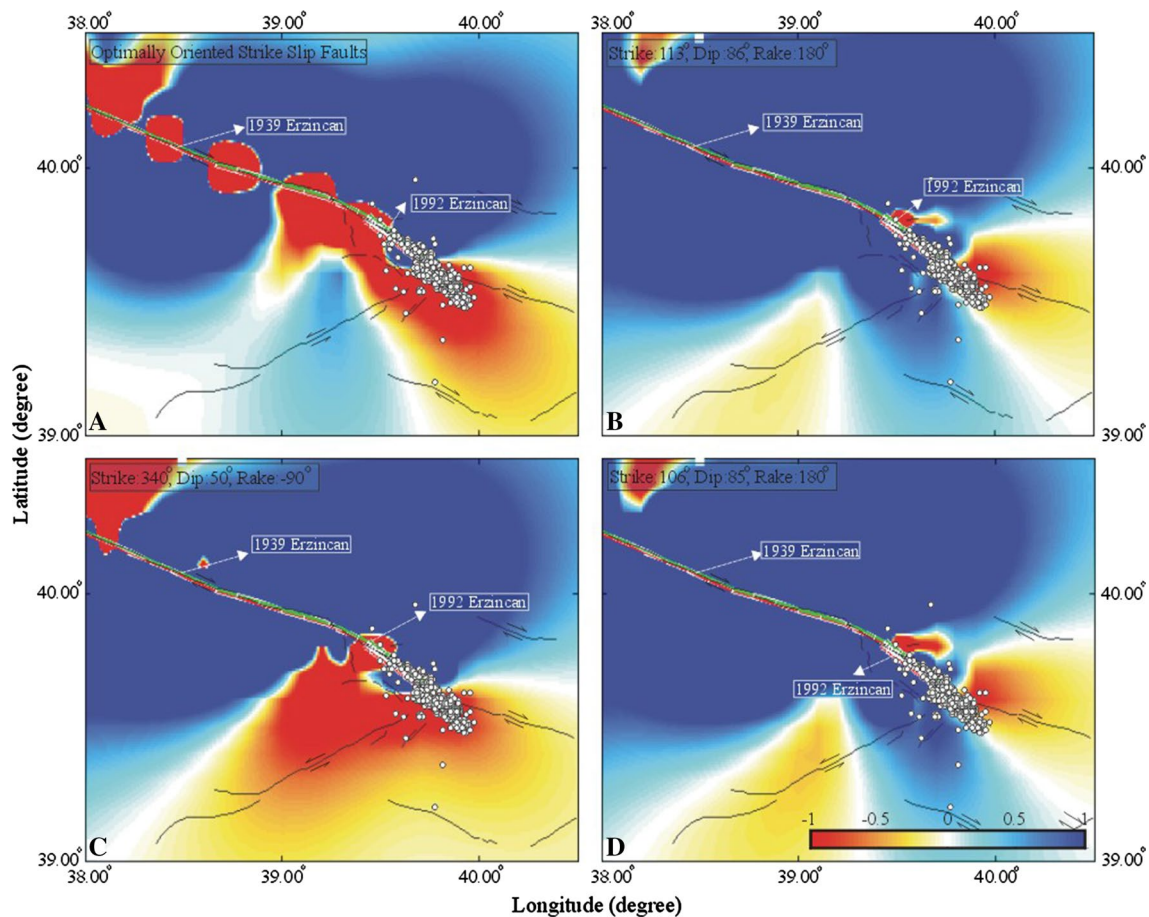


Fig. 6 Coulomb failure stress changes resulting from both the 26 December 1939 and 13 March 1992 Erzincan earthquakes at depth of 8 km. Note that the stress changes resolved onto **a** the optimally oriented strike-slip faults indicate stress increase at the both rupture terminations of the 1992 Erzincan earthquakes while the stress changes resolved onto **b** the easternmost fault segment (strike = 113° , dip = 86° and rake = 180°) of the 1939 Erzincan earthquake and **c** the normal faults (strike = 340° , dip = 50° and rake = -90°) bounding the NW edge of the Erzincan basin require the stress increase at

the western rupture termination of the 1992 Erzincan earthquake virtually to vanish. **d** The stress changes over the Yedisu fault segment (strike = 106° , dip = 85° and rake = 180°) indicate that the receiver fault was stress-loaded by both earthquakes, but the eastern aftershock cluster hardly overlaps with the stress-loaded area and partly falls into the stress shadow (see also Fig. 5d). White circles indicate the aftershocks compiled from Kaypak and Eyidoğan (2005) and Kalafat et al. (2007), and active faults traces are from MTA (2012). See Table 2 for the rupture parameters used in the stress computations

imparted by both earthquakes over the optimally oriented strike-slip faults. The faults mapped in the west of the 1992 earthquake rupture are the easternmost fault segment (strike = 113° , dip = 86° and rake = 180°) of the 1939 Erzincan earthquake and the approximately NS-trending normal faults (strike = 340° , dip = 50° and rake = -90°) along the NW edge of the Erzincan Basin as in the SE margin (MTA 2012). The stress changes estimated over these faults are shown in Fig. 6b, c, respectively. The stress changes in the 1939 and 1992 Erzincan earthquakes over the Yedisu fault segment (strike = 106° , dip = 85° and rake = 180°) are depicted in Fig. 6d.

We have estimated Coulomb stress changes caused by the 1997 Qa'emat earthquake alone as shown in Fig. 7. Figure 7a, b represents the stress changes for the optimally

oriented strike-slip and thrust faults, respectively, along with the 45-day-long available aftershock activity. Regional stress direction used is the same as in 1979 Khuli-Boniabad earthquake and is adapted from Durmuş (2014). Figure 7c, d shows the stress changes over specified rupture planes regarding the available source mechanism solution of the two aftershocks (Berberian et al. 1999). One of these aftershocks (16 June 1997 aftershock, $M_w = 5.0$) occurred at the southern tip of the 1997 Qa'emat earthquake rupture, the source mechanism of which suggests thrust faulting (strike = 120° , dip = 20° and rake = 90°), roughly coinciding also with some mapped subparallel thrust fault extending conjugate to the Abiz fault in the south (Fig. 2d). The other one is the 25 June 1997 aftershock ($M_w = 5.7$), which was located near the junction of the Dasht-e-Bayaz

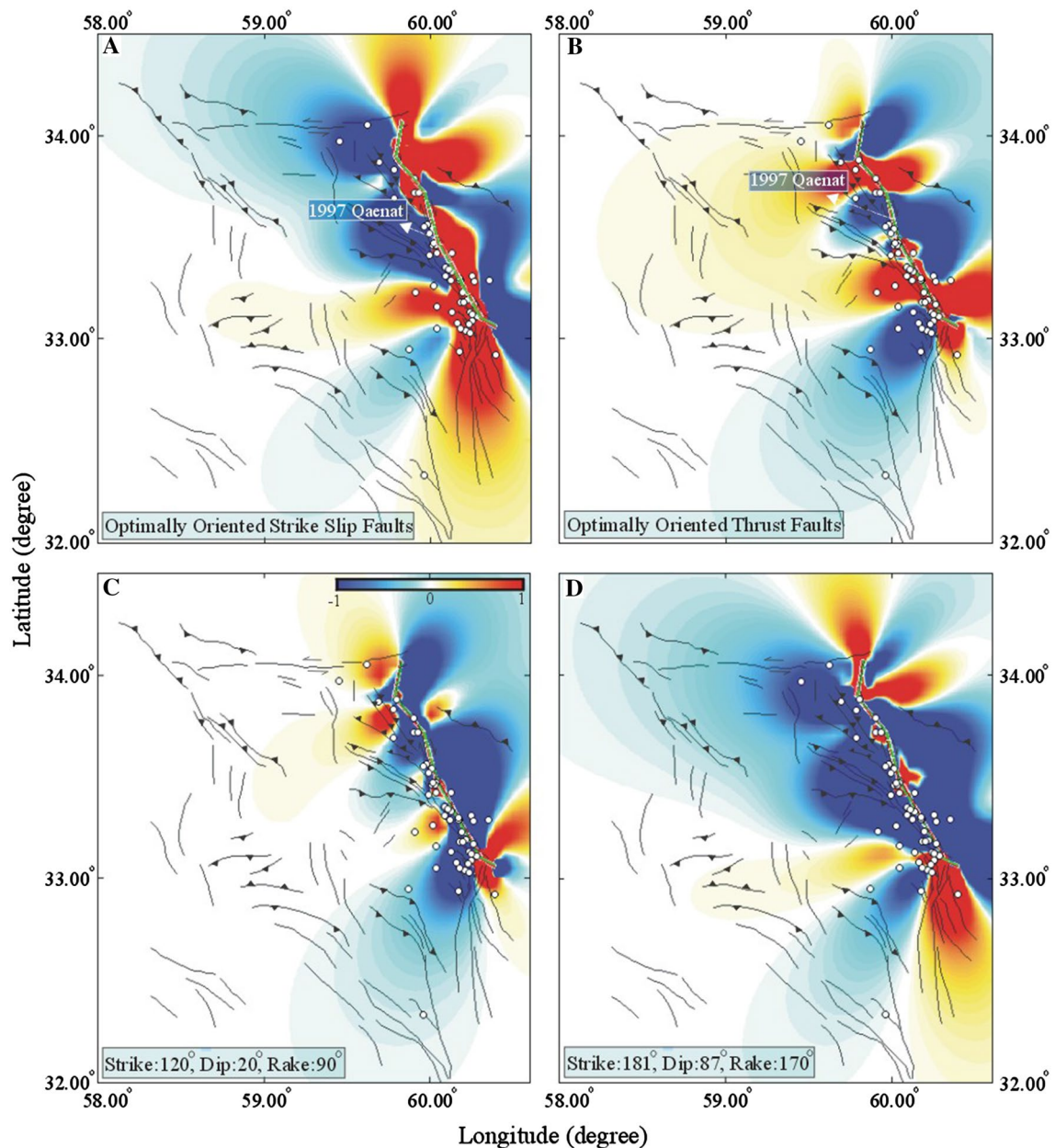


Fig. 7 Stress changes after the 10 May 1997 Qa'enaat earthquake alone together with the 45-day-long aftershocks distribution (*white circles*). The stress changes are resolved onto the optimally oriented **a** strike-slip and **b** thrust faults and resolved onto the two specified rupture planes with **c** strike of 120°, dip of 20° and rake of 90° and

with **d** strike of 181°, dip of 87° and rake of 170°. The aftershocks are compiled from Walker et al. (2011) and USGS-NEIC catalogue and active faults traces are from Berberian et al. (1999). The stress variations are sampled at depth of 8 km. See Table 2 for the rupture parameters used in the stress computations

and Abiz faults where there are several roughly NS-striking strike-slip faults. The source mechanism of the later aftershock indicates strike-slip faulting (strike = 181°, dip = 87° and rake = 170°) (Fig. 2d).

In Fig. 8a, the stress changes due to the background seismicity before the 1997 Qa'enaat earthquake are shown along with the aftershocks. The 1997 Qa'enaat earthquake is added to the background seismicity to calculate stress changes as

depicted in Fig. 8b. The stress changes in Fig. 8a, b are resolved onto the optimally oriented strike-slip faults. Figure 8c, d shows the stress changes as in Fig. 8a, b, respectively, but stress changes have been computed over the optimally oriented thrust faults.

Stress changes caused by the 2006 Silakhor earthquake have been compared with the three-month-long aftershock distribution in Fig. 9a. Figure 9b shows stress changes

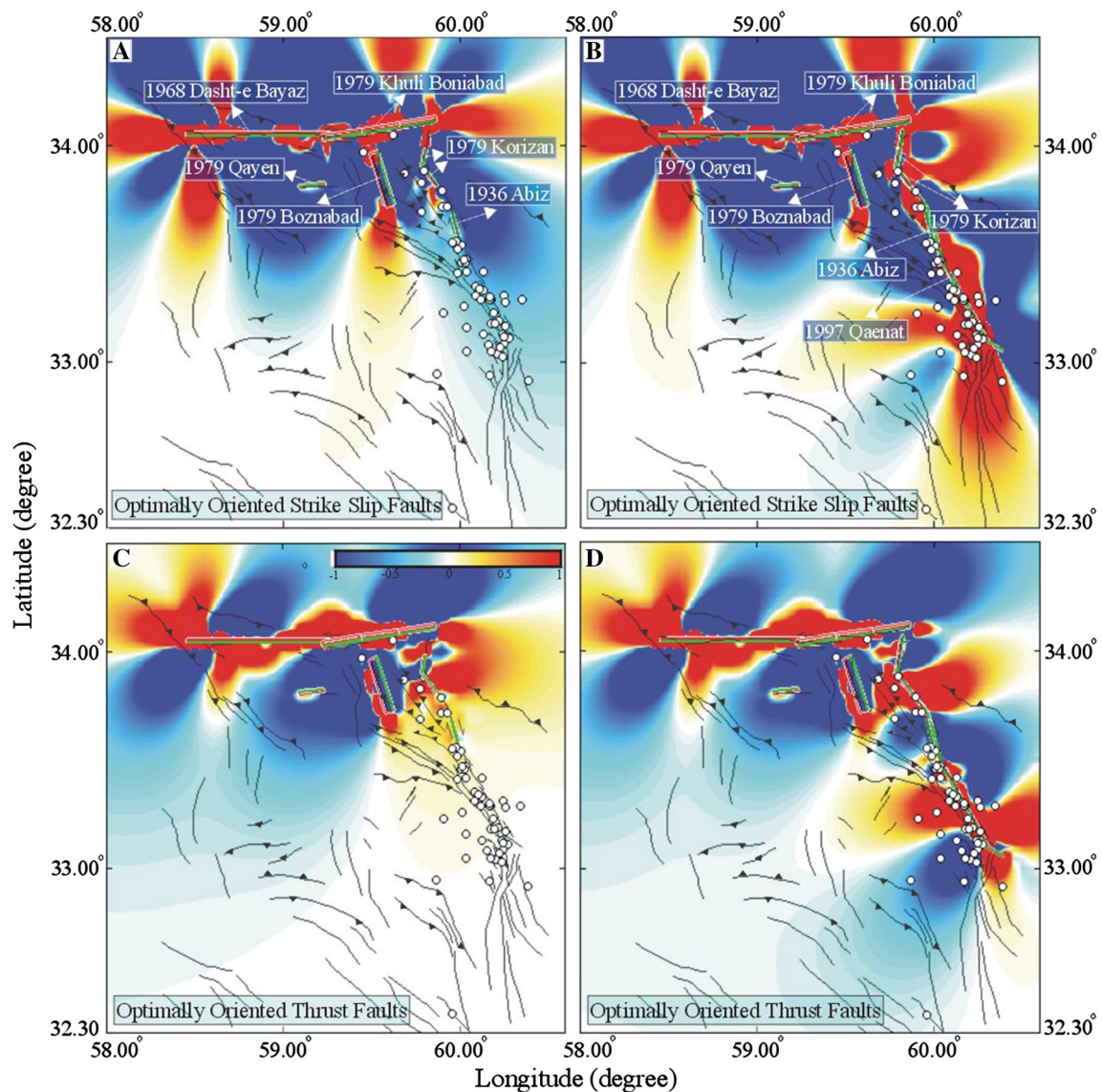


Fig. 8 Stress changes before (maps in the left) and after (maps in the right) the 10 May 1997 Qa'eenat earthquake together with its 45-day-long aftershock distribution (white circles). The stress changes are resolved onto the optimally oriented **a**, **b** strike-slip and **c**, **d** thrust

faults. The maps reflect stress variations at depth of 8 km. See caption of Fig. 7 for the sources from which aftershocks and active faults traces are compiled and Table 2 for the rupture parameters used in the stress computations

imposed by the 2006 Silakhor and two background earthquakes along the Main Recent Fault, the 1909 Lurestan and 1958 Firuzabad earthquakes. Both stress changes have been estimated over the optimally oriented strike-slip faults using regional stress direction given by Zarifi et al. (2013).

Discussion

Coulomb stress modelling studies for the last three decades have demonstrated that there is a general correlation between the stress perturbations caused by mainshocks and aftershock distributions (King et al. 1994; Nalbant et al.

1996; Steacy et al. 2004, 2005; King 2007). Aftershocks generally tend to occur on favourably oriented fault planes close to failure in the region of stress increase following a mainshock. Strike-slip earthquakes have been characterized by static stress-increased lobes and, in general, the clusters of aftershock at both ends of the rupture (King et al. 1994; Stein 2003; Das and Henry 2003; King 2007). However, there have been some cases that the aftershock clusters observed only at the one end or in some cases no report of the aftershocks at the both ends at all (Das and Henry 2003). The mainshock–aftershock sequences studied in the present study give some clues to discuss cause of the one-sided aftershock patterns.

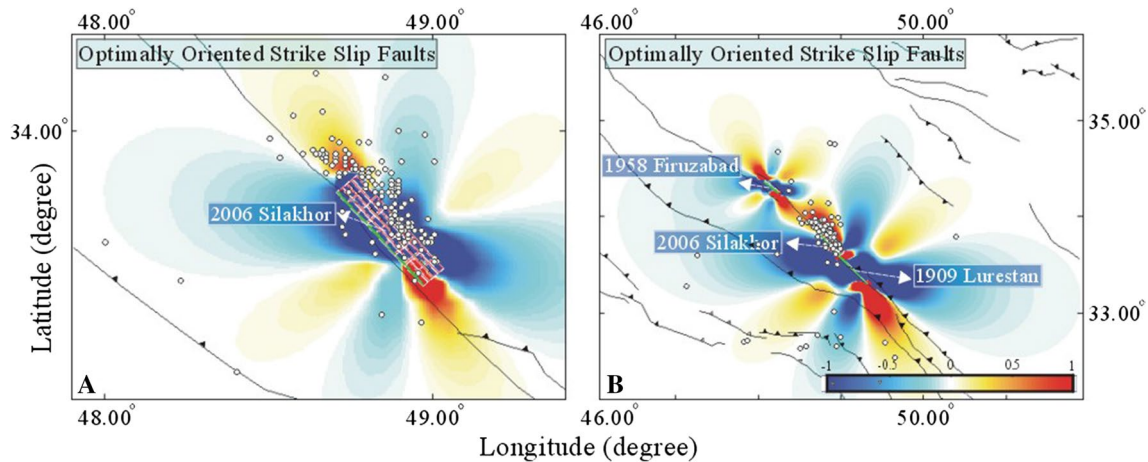


Fig. 9 **a** Stress changes caused by the 31 March 2006 Silakhor earthquake at depth of 8 km have been compared with the three-month-long aftershocks distribution (*white circles*). **b** Stress changes imposed by the 2006 Silakhor and two background earthquakes along the Main Recent Fault, the 1909 Lurestan and 1958 Firuzabad earth-

quakes together with the aftershock distribution. Both stress changes have been estimated over the optimally oriented strike-slip faults. The aftershocks and active faults traces are from IIEES and Ghods et al. (2012), respectively. See Table 2 for the rupture parameters used in the stress computations

As mentioned above, five strike-slip earthquake ruptures are documented to have aftershocks only or mainly one end of their ruptures though they promoted static stresses at both ends of their ruptures, as indicated in Figs. 3a, 4a, 5a, 7a and 9a. Why aftershocks sparsely occurred at the one end would be an interesting and significant question as the Coulomb stress maps have been put forward to comment on the most likely region aftershocks to strike for earthquake hazard mitigation purposes. In search for an answer to this question, influence of the background seismicity has been taken into account. It is realized that all of the mainshocks have been preceded by large earthquake ruptures at their rupture ends with no aftershock observations or a few aftershock occurrence while no background large earthquake rupture at the other ends with abundant aftershock observations.

For the case of the 1979 Imperial Valley earthquake sequence, the relatively strong aftershock distribution exhibits a clear one-sided pattern (Fig. 2a). Though the whole activity without any magnitude threshold seems to be double-sided at first glance, the activity is still one-sided because the NC is much stronger and higher in number as compared to the SC. In addition, the SC is beyond the SE end of the rupture, while the NC covers northernmost section of the rupture and extends towards the Salton Sea. Neither stress distributions in Fig. 3a or b explain well the aftershock of the 1979 Imperial Valley earthquake. Remember that these maps reflect stresses mapped over the planes parallel to the Imperial fault (strike = 143° , dip = 90° and rake = 180°) resulted from the 1979 Imperial Valley earthquake and the background earthquakes. The NC over the BSZ partly falls into the increased stress area, while MC

along the Imperial fault and the SC over the CPSZ completely or mostly fall into the stress-decreased areas. Notice that the SC is mainly outside of the stress-increased lobe in the south-east of the rupture. The most stressed part of the lobe is mostly avoid of the aftershocks, while almost half of the NC fall into the most stressed part of the north-west stress-increased lobe. Figure 3b shows a clue for why the south-east stress-increased lobe is mostly avoid of aftershocks. The Imperial fault beyond the SE end of the 1979 ruptures under the stress decrease due to the background earthquakes, the 1940 Imperial Valley earthquake in particular, suggesting that the stress increase caused by the 1979 earthquake did not overcome the stress shadow of the background earthquakes in that section. When the stress variations estimated over the structures (normal faults with strike = 185° , dip = 50° and rake = -90° and conjugate left-lateral faults with strike = 233° , dip = 66° and rake = -22°) related to the BSZ and CPSZ (Fig. 3c–f), it is seen that both stress changes caused by the 1979 Imperial Valley earthquake alone and along with the all background earthquakes correlate well with the aftershock clusters over the seismic zones in the ends of the rupture with the exception of the MC, which still falls into the stress-decreased area along the Imperial fault. Note the merely absence of the aftershocks related to the SC in the most stressed area of the south-east stress-increased lobe both in Fig. 3c, e as contrary to the aftershocks related to the NC, which mainly falls into the most stressed area of the north-west stress-increased lobe. Stress changes maps shown in Fig. 3d, f indicate that the background earthquake ruptures strongly promoted stresses over the CPSZ while decreasing stresses between the SE end of the 1979 Imperial Valley earthquake

rupture and the main body of the SC, providing a reasonable explanation for the observed aftershock pattern in the SE.

A NE–SW-trending elongated aftershock zone within the NC and just NW of the 1979 Imperial Valley earthquake rupture is clearly separable indicating that one of the left-lateral fault conjugate to the Imperial fault in the south of the Salton Sea was activated by the stress transfer caused by the earthquake (Johnson and Hutton 1982; Fuis et al. 1982) (Figs. 2a, 3e, f). The fact that this fault produced the 2012 Brawley earthquake swarm (Hauks-son et al. 2013) supports not only its presence and active character but also its possible activation due to the stress transfer by the 1979 Imperial Valley earthquake. The MC falls into the stress shadow in the stress maps in Fig. 3a–f. When the stress changes are calculated over the optimally oriented faults (Fig. 3g), the MC is still inside the stress shadow of the 1979 Imperial fault. Nevertheless, the background earthquakes caused stress load in the area of the MC (Fig. 3h), which is located over a geothermal area (Fuis et al. 1982). Majority of the MC consists of $M < 3.0$ aftershocks as it is clearly shown in Figs. 2a and 3h, indicating that this cluster was a product of very heterogeneous crustal volume with differently oriented cracks surrounding that part of the Imperial fault resulting from the geothermal activity. Dynamic stress triggering could also be considered as the cause behind the MC activity because dynamic stresses do not have stress shadows and the heterogeneous crustal volume may provide proper condition for dynamic stress triggering.

As shown in Fig. 4a, there was no aftershock beyond the western end of the 1979 Khuli-Boniabad earthquake rupture within the western stress-increased lobe while there were several aftershocks along and just beyond its eastern end within eastern stress-increased lobe, including the largest aftershock, namely the 7 December 1979 Kalat-e-Shur earthquake (Fig. 2b). When the stresses imparted by the large earthquakes back in the time are taken into the account, the stress-increased lobe of the 1979 Khuli-Boniabad earthquake in the west gets significantly suppressed by the stress shadow of the 1968 Dasht-e-Bayaz earthquake (Fig. 4b). The suppression becomes more apparent as the stress is computed over the 1968 Dasht-e-Bayaz earthquake fault plane (Fig. 4c). It seems that the stress shadow of the 1968 Dasht-e-Bayaz earthquake had not faded away enough in the time period between 1968 and 1979 to be fully overcome by the coseismic stress increases exerted by the 1979 Khuli-Boniabad earthquake, causing absence of the aftershocks in the west.

The stress map for optimally oriented strike-slip fault in Fig. 5a explains the 1992 Erzincan earthquake aftershock distribution fairly well. However, the aftershocks just beyond the eastern rupture termination (corresponds to

the aftershock zones 2–4 of Fuenzalida et al. (1997)) fall into the stress-decreased area. These aftershocks fault plane solutions suggest EW-trending extension, which requires normal faulting along roughly NS-striking normal faults (Fuenzalida et al. 1997; Grosser et al. 1998) as expected for the fault stepover between the ES and Yedisu segment (Fig. 2c). A stress change calculation along rupture planes representing (strike = 192° , dip = 50° and rake = -86°) those normal faults, the representative rupture parameters of which have been approximately deduced from the results of stress tensor inversion of the respective aftershock clusters by Fuenzalida et al. (1997), reveals stress increase for that area (Fig. 5b). This means that almost all of the eastern aftershock cluster fall into the stress enhancement area regarding both Fig. 5a, b.

The aftershock distribution of the 1992 Erzincan earthquake elongated in NW–SE direction and the elongation becomes more pronounced in its easternmost part (Fig. 2c). That part has been related to the rupture growth of the largest aftershock, the 1992 Pülümür earthquake, by Fuenzalida et al. (1997). The strike of the aftershock elongation (about 130°) differs almost 30° from the strike of the Yedisu fault segment and coincides quite well with extend of the Pülümür fault (Fig. 2c) (MTA 2012). The Pülümür fault strikes more southerly as it goes to the east and its strike varies from 110° to 130° . Plus, the eastern extreme of the aftershock cluster and change in its strike from east to west exactly fit to the end and strike change in the Pülümür fault, respectively, and SW dipping nodal plane (strike = 129° , dip = 43° and rake = 134°) from the source mechanism by Fuenzalida et al. (1997) coincides with the strike of the fault, considering its epicentral location (Fig. 2c). Both the epicentre of the 1992 Pülümür earthquake and the easternmost part of the aftershock cluster fall south of the Pülümür fault, supporting a south-west dipping rupture plane. Figure 5c shows stress changes map over the fault planes parallel to the Pülümür fault. When the stress changes resolved onto the Yedisu fault segment (strike = 106° , dip = 85° and rake = 180°) (Fig. 5d), it is seen that the eastern lobes of stress increase beyond the mainshock rupture in both Fig. 5a, c are in a better agreement with the off-fault aftershock cluster as compared to Fig. 5d. Note that the strike of the Pülümür fault closely corresponds to the optimally oriented dextral failure planes. All these findings support that it is much likely that the largest 1992 Pülümür aftershock and the easternmost aftershock cluster to be generated by the Pülümür fault rather than the left-lateral and NE–SW-striking Ovacık fault zone as previously thought (Nalbant et al. 1996; Fuenzalida et al. 1997). The Coulomb failure stresses imparted by the 1992 Erzincan earthquake might have activated the Pülümür fault.

Why there is virtually no aftershock at the western termination of the 1992 Erzincan earthquake rupture as

compared to a large cluster of off-fault aftershocks at the other end is the question we focus on now. Note that there is a considerable stress-increased area not only at the eastern termination of the 1992 Erzincan earthquake rupture plane but also at the western end, along the optimally oriented strike-slip faults (Fig. 6a). This contradicts with no observation of the off-fault aftershocks at the western rupture termini of the 1992 Erzincan earthquake. Therefore, the stress changes are calculated over the specified fault planes (Fig. 6b, c). Figure 6b shows a stress shadow beyond the western rupture termination of the 1992 Erzincan earthquake rupture along the easternmost fault segment of the 1939 Erzincan earthquake rupture. The stress shadow still persists when stress changes are sampled along the normal faults at the NW edge of the Erzincan basin (Fig. 6c). These suggest that the faults that would be possible source of the aftershocks in the west of the 1992 Erzincan earthquake rupture had been strongly relaxed by the 1939 Erzincan earthquake stress shadow, which was not overcome by the stress-increased lobe caused by the 1992 Erzincan earthquake rupture after about 50 years. In other words, the aftershock distribution of the 1992 Erzincan earthquake has been suppressed by the stress shadow resulting from the 1939 Erzincan earthquake. This has been underlined by Nalbant et al. (1996) as well. Also note that though optimally oriented strike-slip fault planes under stress increase there is no optimally oriented mapped strike-slip faults to response as aftershock occurrences in the west. The existent fault planes are under stress shadow, demonstrating control of aftershock occurrences by the existing structures (McCloskey et al. 2003; Steacy et al. 2005). Note that though the Yedisu fault segment (strike = 106° , dip = 85° and rake = 180°) is strongly stress-loaded by the 1939 Erzincan earthquake as indicated in Fig. 6d and the aftershocks are mostly located between stress-increased and stress-decreased lobes in the SW of the segment (Fig. 6d). Considering that the Yedisu Fault segment has not ruptured since 1784 and is a seismic gap, it is reasonable to claim that the segment is locked and has become much closer to failure after both of the Erzincan earthquakes. Recent studies (Reilinger et al. 2006; Cakir et al. 2014) have indicated that the slip rate along the segment about 20–25 mm/year. This means that about 5.5–6 m of slip accumulated along the segment after 1784 and the segment is currently capable of producing at least $M_w = 7.4$ earthquake, the occurrence of which has been quickened by the stress load of both 1939 and 1992 Erzincan earthquakes.

The stress changes maps for the 1997 Qa'emat earthquake shown in Fig. 7 suggest that the aftershock distribution is well explained by the stress changes resolved onto the optimally oriented strike-slip and thrust faults (Fig. 7a, b), considering the type of the nearby active faults (Fig. 2d). The aftershocks mostly occurred in the

stress-increased lobes in the south and south-west of the 1997 Qa'emat earthquake rupture, while there is no aftershock in the stress-increased lobe in the north and north-east of the rupture. Several aftershocks that fall into the stress shadow area in Fig. 7a in the west of the 1997 Qa'emat earthquake rupture between 1936 Abiz and 1979 Korizan earthquakes ruptures fall into stress-increased area when the stress changes are resolved onto the optimally oriented thrust faults (Fig. 7b). Because, active fault maps indicate NW–SE-trending subparallel thrust faults in that area (Berberian et al. 1999) (Fig. 2d). The stress changes due to the background large earthquakes over the optimally oriented strike-slip faults indicate that both sides of the northern half of the 1997 Qa'emat earthquake rupture mostly under strong stress shadow compared to the southern half that is under a weak stress shadow (Fig. 8a). The past earthquakes imposed a stress-increased lobe in the east of the 1979 Khuli-Boniabad earthquake rupture. When the 1997 Qa'emat earthquake rupture along with the past earthquakes is included in the stress estimates, it is obtained that stress shadow gets much broader towards south especially to the south-east for the strike-slip faults while two stress-increased lobes appear around the southern extreme of the rupture (compare Fig. 7a with 8a). The stress-increased lobe of the 1997 Qa'emat earthquake in the northeast partly turns a stress-decreased area close to the Abiz fault due to the background earthquake ruptures (Fig. 8b). The stress shadow of the past earthquakes around the northern half of the 1997 Qa'emat earthquake rupture seems to be not fully overwhelmed by the 1997 Qa'emat earthquake's stress changes, explaining relatively rare occurrence of the aftershocks around the northern half of the rupture as compared to the southern half. However, the stress shadow towards the south rupture extreme is not strong enough and has been overwhelmed by the 1997 Qa'emat earthquake stress increase, resulting in most of the aftershocks. Note that the stress changes over the optimally oriented thrust faults due to the background earthquakes require mostly stress enhancement around the northern half of the rupture (Fig. 8c). Though the stress enhancement area became smaller following the 1997 Qa'emat earthquake (Fig. 8d), it coincides with the several aftershock occurrences that fall into the stress shadow in Fig. 8a, b. These findings suggest not only that the aftershock occurrences are controlled by the structures but also that the stress changes in the past background earthquakes and their coincidence with the stress changes in the current mainshock might influence the pattern of the aftershock sequence.

As shown in Fig. 9a, 2006 Silakhor earthquake rupture and its aftershock distribution resembles the 1992 Erzincan earthquake rupture and its aftershock pattern with an aftershock cluster only over a stress-increased lobe beyond the NW rupture termini. Figure 9b shows that the stress

changes caused by the two background large earthquakes promote the stresses along and beyond the rupture of the 2006 Silakhor earthquake while they require stress decrease over the stress lobe beyond the SE rupture termini. The stress shadow of the 1909 Lurestan earthquake in the SE neighbourhood seems to be not overcome by the coseismic stress increase in the 2006 Silakhor earthquake resulting in unfavourable condition for the aftershock occurrence or halting of aftershock seismicity. However, the NW stress-increased lobe of the 2006 Silakhor earthquake overlapped with the 1909 Lurestan earthquake's stress increase in the north of its rupture and the 1958 Firuzabad earthquake's southern stress-increased lobe, providing favourable condition for the aftershock occurrence. Compared to the 1909 Lurestan earthquake rupture in the SE, the 1958 Firuzabad earthquake rupture is far away to cause stress decrease along and beyond the 2006 Silakhor earthquake rupture. Therefore, the 2006 Silakhor earthquake sequence exemplifies influence of the background stress field on the aftershock pattern of the later mainshocks.

The five cases of the aftershock sequences in the strike-slip fault environments presented in the study suggest that either the stress shadows or stress-increased areas resulting from large background earthquakes occurred decades before play a significant role in the spatial distribution of the aftershocks of the later shocks. It seems that the stress shadows from the large background earthquakes persist for decades to suppress the aftershocks occurrence of the current large earthquakes such that there is a few or absence of aftershocks in the crustal volumes with stress decrease. The 1979 Imperial Valley and 1992 Erzincan earthquakes exemplify not only the effect of the background stress shadows on the current aftershock patterns but also influence of the stress-increased areas from the earthquakes in the background. It is also important to note the stress changes from the background earthquakes playing a key role in the location of the largest aftershocks. With the exception of the 1997 Qa'emat earthquake, for the all studied earthquakes the largest aftershocks did not occur at the rupture ends influenced by the stress shadows of the earthquakes in the near past (compare Figs. 2a with 3h, 2b with 4b, 2c with 6b, and 2e with 9b).

It is now well known that the post-seismic deformations can further alter the static stresses in the upper crust from several days to many decades in respond to large earthquakes. These post-seismic mechanisms are classically divided into three: (1) after slip which involves transient deformations on the generating fault following a large earthquake. This afterslip usually occurs in areas of low seismic slip, where the fault zone was loaded during the earthquake (Marone et al. 1991); (2) poroelastic rebound which is time-dependent poroelastic re-equilibrium occurring close to the rupturing fault (Bosl and Nur 2000); and

(3) the viscoelastic relaxation of the ductile lower crust and upper mantle layers. The first two are affective in short-time scales (days to weeks) mostly and the third one can last many decades depending on the magnitude of the mainshock (Pollitz et al. 1998).

Modelling of the stress changes caused by the post-seismic deformations is out of scope of present paper. They would surely alter the stress field due to the background earthquakes in the upper crust, but it is shown that they are not the first-order mechanisms compared to the elastic coseismic ruptures (Steady et al. 2005). It is also noted that for strike-slip faults, positive stress lobes increase in magnitude owing to viscous relaxation, and regions in which coseismic stress changes were negative tend to get more negative (Freed and Lin 1998; Freed 2005). This means that the stress field created by the background earthquakes can sustain many decades and influence the seismicity pattern of the aftershocks.

All these mean that the stress changes in the past earthquake or earthquakes might be a factor to govern the aftershock spatial distribution of the future earthquake and one of the reasons behind the one-sided aftershock clusters observation. This puts forward that they should be taken into account as an element of the earthquake hazard assessment due to the aftershocks of the current mainshocks. The documented correlations between the stress field and both aftershock seismicity and background seismicity in the past (Nalbant et al. 1998; Toda et al. 2012; Sevilgen et al. 2012) support not only this reckoning but also significance of earthquake stress change maps in assessment of earthquake hazard.

Conclusions

Five mainshock–aftershock sequences taken from different strike-slip fault environments of the globe have been studied by means of the Coulomb static stress changes, also considering the stress changes from the large earthquakes in their backgrounds. The 15 October 1979 Imperial Valley earthquake ($M_w = 6.4$) in southern California, the 27 November 1979 Khuli-Boniabad ($M_w = 7.1$), the 10 May 1997 Qa'emat ($M_w = 7.2$) and the 31 March 2006 Silakhor ($M_w = 6.1$) earthquakes in Iran and the 13 March 1992 Erzincan earthquake ($M_w = 6.7$) in Turkey have been studied because these earthquakes are mainly characterized by one-sided aftershock distributions considering numbers and magnitudes of the aftershocks. We documented that the stress changes resulted from background mainshock(s) that are close in both time and space might be the reason behind the observed aftershock patterns and aftershock occurrences were rare in the strong stress shadows resulting from the background earthquakes, particularly if they

overlap with the stress shadows of the mainshocks under interest. When the stress-increased areas from the background earthquakes coincide with the stress enhancement areas of the current earthquakes, the aftershocks were plenty in numbers in those areas, comprising the largest aftershocks. It is suggested that the stress changes from the previous mainshocks may persist in the crust for decades to influence aftershock distribution of the current mainshocks and they should be taken into account in the usage of the Coulomb stress change maps for earthquake risk mitigation purposes.

Acknowledgments We thank the reviewers for their careful reviews and comments that improved the manuscript. This research was supported by Scientific and Technological Council of Turkey (TUBITAK) postdoctoral fellowship and was partly funded by Research Fund of the Sakarya University (Project Number: 2012-01-14-005).

References

- Aktar M, Dorbath C, Arpat E (2004) The seismic velocity and fault structure of the Erzincan basin, Turkey, using local earthquake tomography. *Geophys J Int* 156:497–505. doi:10.1111/j.1365-246X.2004.02081.x
- Allen CR, Amand PS, Richter CF, Nordquist JM (1965) Relationship between seismicity and geologic structure in the southern California region. *Bull Seism Soc Am* 55(4):753–797
- Ambraseys NN, Melville CP (1982) A history of Persian earthquakes. Cambridge, New York, ISBN 0521 24112 X
- Ambraseys NN, Tchalenko JS (1969) The Dasht-e-Bayaz (Iran) earthquake of August 31, 1968: a field report. *Bull Seism Soc Am* 59(5):1751–1792
- Barka A (1996) Slip distribution along the North Anatolian Fault associated with large earthquakes of the period 1939–1967. *Bull Seism Soc Am* 59:521–589
- Berberian M, Yeats RS (1999) Patterns of historical earthquake rupture in the Iranian Plateau. *Bull Seism Soc Am* 89(1):120–139
- Berberian M, Jackson JA, Qorashi M et al (1999) The 1997 May 10 Zirkuh (Qa' enat) earthquake (M_w 7.2): faulting along the Sistan suture zone of eastern Iran. *Geophys J Int* 136:671–694
- Bosl WJ, Nur A (2000) Crustal fluids and earthquakes. In: Rundle JB, Turcotte DL, Klein W (eds) *GeoComplexity and the physics of earthquakes*, vol Geophys Monogr Ser 120. AGU, Washington, DC
- Bulut F, Bohnhoff M, Eken T, Janssen C, Kılıç T, Dresen G (2012) The East Anatolian Fault Zone: seismotectonic setting and spatiotemporal characteristics of seismicity based on precise earthquake locations. *J Geophys Res* 117:B07304. doi:10.1029/2011JB008966
- Cakir Z, Ergintav S, Akoğlu AM et al (2014) InSAR velocity field across the North Anatolian Fault (eastern Turkey): implications for the loading and release of interseismic strain accumulation. *J Geophys Res Solid Earth* 119(10):7934–7943. doi:10.1002/2014JB011360
- Chavez D, Gonzales J, Reyes A et al (1982) Mainshock location and magnitude determination using combined U.S. and Mexican data, in The Imperial Valley earthquake of October 15, 1979. *US Geol Surv Profess Paper* 1254:51–54
- Clark MM (1972) Surface rupture along the Cayote Creek fault, in The Borrego Mountain earthquake of April 9, 1968. *US Geol Surv Profess Paper* 787:55–86
- Cocco M, Nostro C, Ekstrom G (2000) Static stress changes and fault interaction during the 1997 Umbria-Marche earthquake sequence. *J Seismol* 4:501–516
- Copley A, Jackson J (2006) Active tectonics of the Turkish-Iranian Plateau. *Tectonics* 25:TC6006. doi:10.1029/2005TC0011906
- Das S, Henry C (2003) Spatial relation between main earthquakes slip and its aftershock distribution. *Rev Geophys* 41:3. doi:10.1029/2002RG000119
- Deng J, Sykes LR (1997) Evolution of the stress field in southern California and triggering of moderate-size earthquakes: a 200-year perspective. *J Geophys Res* 102(B5):9859–9886
- Djamour Y, Vernant P, Nankali HR, Tavakoli F (2011) NW Iran-eastern Turkey present-day kinematics: results from the Iranian permanent GPS network. *Earth Planet Sci Lett* 307:27–34
- Doser DI, Olsen KB, Pollitz FF et al (2009) The 1911 $M \sim 6.6$ Calaveras earthquake: source parameters and the role of static, viscoelastic, and dynamic Coulomb stress changes imparted by the 1906 San Francisco Earthquake. *Bull Seism Soc Am* 99(3):1746–1759. doi:10.1785/0120080305
- Durmuş H (2014) İran Depremlerinin Faylanma Özelliklerinin ve Deprem Gerilme Etkileşimlerinin Modellenmesi. PFD Dissertation, Sakarya Üniversitesi
- Freed AM (2005) Earthquake triggering by static, dynamic, and post-seismic stress transfer. *Annu Rev Earth Planet Sci* 33:335–367. doi:10.1146/annurev.earth.33.092203.122505
- Freed AM, Lin J (1998) Time-dependent changes in failure stresses following thrust earthquakes. *J Geophys Res* 103(10):24393–24409
- Freed AM, Ali ST, Bürgmann R (2007) Evolution of stress in Southern California for the past 200 years from coseismic, postseismic and interseismic stress changes. *Geophys J Int* 169:1164–1179
- Fuenzalida H, Dorbath L, Cisternas A et al (1997) Mechanism of the 1992 Erzincan earthquake and its aftershocks, tectonics of the Erzincan Basin and decoupling on the North Anatolian Fault. *Geophys J Int* 129:1–28
- Fuis GS, Money WD, Healey JH et al (1982) Crustal structure of the Imperial Valley Region, in The Imperial Valley earthquake of October 15, 1979. *US Geol Surv Profess Paper* 1254:25–49
- Gheitanchi MR, Zarifii Z (2004) Investigation of upper crust anisotropy in Ghaen-Birjand region, east-central Iran. *Acta Seismol Sin* 17(5):518–525. doi:10.1007/s11589-004-0033-1
- Ghods A, Rezapour M, Bergman E et al (2012) Relocation of the 2006 M_w 6.1 Silakhour, Iran, Earthquake sequence: details of fault segmentation on the main recent fault. *Bull Seism Soc Am* 102(1):398–416. doi:10.1785/0120110009
- Grosser H, Boumbach M, Berckhemer H et al (1998) The Erzincan (Turkey) Earthquake (M_s 6.8) of March 13, 1992 and its Aftershock Sequence. *Pure Appl Geophys* 152:465–505
- Haghipour A, Amadi M (1980) The November 14 to December 25, 1979, Ghaenat earthquakes of northeast Iran and their tectonic implications. *Bull Seism Soc Am* 70:1751–1757
- Hamzehloo H, Rahimi H, Sarkar I et al (2009) Modeling the strong ground motion and rupture characteristics of the March 31, 2006, Darb-e-Astane earthquake, Iran, using a hybrid of near-field SH-wave and empirical Green's function method. *J Seismol* 14:169–195. doi:10.1007/s10950-009-9159-x
- Harris RA (1998) Introduction to special section: stress triggers, stress shadows, and implication for seismic hazard. *J Geophys Res* 103:24347–24358
- Hartzell SH, Heaton TH (1983) Inversion of strong ground motion and teleseismic waveform data for the fault rupture history of the 1979 Imperial Valley, California, earthquake. *Bull Seism Soc Am* 73(6):1553–1583
- Harvard GCMT Global CMT Catalog Search. <http://www.globalcmt.org/CMTsearch.html>. Accessed 10 Jan 2015

- Hauksson E, Stock J, Bilham R et al (2013) Report on the August 2012 Brawley earthquake swarm in Imperial Valley, southern California. *Seism Res Lett* 84(2):177–189. doi:10.1785/0220120169
- Heidbach O, Tingay M, Barth A et al (2008) The World Stress Map database release. doi:10.1594/GFZ.WSM.Rel2008
- Hessami K, Jamali F, Tabassi H (2003) Major Active Faults of Iran (map), scale 1:2,500,000, Ministry of Science Research and Technology International Institute of Earthquake Engineering and Seismology IIEES
- Hutton K, Woessner J, Hauksson E (2010) Earthquake monitoring in southern California for seventy seven years (1932–2008). *Bull Seism Soc Am* 100(2):423–446. doi:10.1785/0120090130
- IIEES International Institute of Earthquake Engineering and Seismology. www.iiees.ac.ir/en/. Accessed 10 Jan 2015
- Ikeda Y, Imaizumi T, Sato H et al (1999) Surface faults associated with the Qayen, northeast Iran, earthquake of May 10, 1997. *Active Fault Res* 18:1–13
- Jackson J (1992) Partitioning of strike-slip and convergent motion between Eurasia and Arabia in eastern Turkey. *J Geophys Res* 97:12471–12479
- Johnson CE, Hadley D (1976) Tectonic implications of the Brawley Earthquake Swarm, Imperial Valley, California, January 1975. *Bull Seism Soc Am* 66(4):1133–1144
- Johnson CE, Hill DP (1982) Seismicity of the Imperial Valley, in the Imperial Valley earthquake of October 15, 1979. *US Geol Surv Profess Paper* 1254:15–24
- Johnson CE, Hutton LK (1982) Aftershocks and Preearthquake Seismicity, in The Imperial Valley earthquake of October 15, 1979. *US Geol Surv Profess Paper* 1254:59–76
- Kalafat D, Günes Y, Kara M et al (2007) A revised and extended earthquake catalogue for Turkey since 1900 (M4.0). Boğaziçi University, Kandilli Rasathanesi ve Deprem Araştırma Enstitüsü, İstanbul
- Kassarasa KV, Karakonstantis A, Kaviris G et al (2014) The April–June 2007 Trichonis Lake earthquake swarm (W. Greece): new implications toward the causative fault zone. *J Geodyn* 73:60–80
- Kaypak B (2008) Three-dimensional Vp and Vp/Vs structure of the upper crust in the Erzincan basin (eastern Turkey). *J Geophys Res* 113:B07307. doi:10.1029/2006JB004905
- Kaypak B, Eyidoğan H (2005) One-dimensional crustal structure of the Erzincan basin, Eastern Turkey and relocations of the 1992 Erzincan earthquake (Ms = 6.8) aftershock sequence. *Phys Earth Planet Inter* 151:1–20
- King GCP (2007) Fault interaction, earthquake stress changes, and the evolution of seismicity. *Treatise Geophys* 4:225–255
- King GCP, Stein RS, Lin J (1994) Static stress changes and the triggering of earthquakes. *Bull Seism Soc Am* 84(3):935–953
- Lasocki S, Karakostas VG, Papadimitriou EE (2009) Assessing the role of stress transfer on aftershock locations. *J Geophys Res* 114:B11304. doi:10.1029/2008JB006022
- Lin J, Stein RS (2004) Stress triggering in thrust and subduction earthquakes and stress interaction between the southern San Andreas and nearby thrust and strike-slip faults. *J Geophys Res* 109:B02303. doi:10.1029/2003JB002607
- Lin J, Stein RS, Meghraoui M et al (2011) Stress transfer among en echelon and opposing thrusts and tear faults: triggering caused by the 2003 Mw = 6.9 Zemmouri, Algeria, earthquake. *J Geophys Res* 116:B03305. doi:10.1029/2010JB007654
- Marone CJ, Scholtz CH, Bilham R (1991) On the mechanics of the earthquake afterslip. *J Geophys Res* 96(5):8441–8452
- McCloskey J, Nalbant SS (2009) Near-real-time aftershock hazard maps. *Nat Geosci* 2:154–155
- McCloskey J, Nalbant SS, Steacy S, Nostro C, Scotti O, Baumont D (2003) Structural constraints on the spatial distribution of aftershocks. *Geophys Res Lett*. doi:10.1029/2003GL017225
- McClusky S, Balassanian S, Barka A et al (2000) GPS constraints on plate kinematics and dynamics in the Eastern Mediterranean and Caucasus. *J Geophys Res* 105:5695–5719
- Meltzner AJ, Rockwell TK, Owen LA (2006) Recent and long-term behavior of the Brawley Fault Zone, Imperial Valley, California: an escalation in slip rate? *Bull Seism Soc Am* 96(6):2304–2328
- Mouthereau F, Lacombe O, Verges J (2012) Building the Zagros collisional orogen: timing, strain distribution and the Dynamics of Arabia/Eurasia plate convergence. *Tectonophysics* 532–535:27–60. doi:10.1016/j.tecto.2012.01.022
- MTA (2012) Türkiye Yenilenmiş Diri Fay Haritası. <http://www.mta.gov.tr/v2.0/default.php?id=yenidirifayharitalari-goruntule>. Accessed 19 June 2013
- Nalbant SS, Barka AA, Alptekin Ö (1996) Failure stress change caused by the 1992 Erzincan earthquake (Ms = 6.8). *Geophys Res Lett* 23:1561–1564
- Nalbant SS, Hubert A, King GCP (1998) Stress coupling between earthquakes in northwest Turkey and the north Aegean Sea. *J Geophys Res* 103(B10):24469–24486
- Nalbant SS, McCloskey J, Steacy S, Barka AA (2002) Stress accumulation and increased seismic risk in eastern Turkey. *Earth Planet Sci Lett* 195:291–298
- Okada Y (1992) Internal deformation due to shear and tensile faults in a half-space. *Bull Seism Soc Am* 82(2):1018–1040
- Parsons T (2004) Recalculated probability of $M \geq 7$ earthquakes beneath the Sea of Marmara, Turkey. *J Geophys Res* 109:B05304. doi:10.1029/2003JB002667
- Peyret M, Rolandone F, Dominguez S et al (2008) Source model for the Mw 6.1, 31 March 2006, Chalan-Chulan Earthquake (Iran) from InSAR. *Terra Nova* 20(2):126–133. doi:10.1111/j.1365-3121.2008.00797.x
- Pınar A, Hokura Y, Kikuchi M (1994) Rupture process of the 1992 Erzincan earthquake and its implication for seismotectonics in eastern Turkey. *Geophys Res Lett* 21:1971–1974
- Pollitz FF, Bürgmann R, Segall P (1998) Joint estimation of afterslip rate and postseismic relaxation following the 1989 Loma Prieta earthquake. *J Geophys Res* 103(11):26975–26992
- Raju PS, Gahalaut VK, Ravi KM (2008) Phodong (Sikkim) earthquake of 14 February 2006 and its aftershocks-Coulomb stress analysis. *J Geodyn* 46:63–67
- Ramazi H, Hosseinnejad M (2009) The Silakhor (Iran) earthquake of 31 March 2006, from an engineering and seismological point of view. *Seismol Res Lett* 80(2):224–232. doi:10.1785/gssrl.80.2.224
- Reilinger R, McClusky S, Vernant P et al (2006) GPS constraints on continental deformation in the Africa-Arabia-Eurasia continental collision zone and implications for the dynamics of plate interactions. *J Geophys Res* 111:B05411. doi:10.1029/2005JB004051
- Rezapour M (2009) Analysis of the causative fault during Silakhor earthquake, March 31, 2006 in Lorestan province. *Iran J Geophys* 3(1):75–89
- Rockwell TK, Klinger Y (2013) Surface rupture and slip distribution of the 1940 Imperial Valley, earthquake, imperial fault, southern California: implications for rupture segmentation and dynamics. *Bull Seism Soc Am* 103(2A):629–640. doi:10.1785/0120120192
- Sandvol E, Türkelli N, Barazangi M (2003) The Eastern Turkey Seismic Experiment: the study of a young continent-continent collision: An example from eastern Turkey. *Geophys Res Lett* 30(24):8038. doi:10.1029/2003GL018912
- Sato T, Hiratsuka S, Mori J (2012) Coulomb stress change for the normal-fault aftershocks triggered near the Japan Trench by the 2011 Mw 9.0 Tohoku-Oki earthquake. *Earth Planets Space* 64:1239–1243
- Sevilgen V, Stein RS, Pollitz FF (2012) Stress imparted by the great 2004 Sumatra earthquake shut down transforms and activated

- rifts up to 400 m away in the Andaman Sea. *Proc Natl Acad Sci* 109(38):15152–15156. doi:[10.1073/pnas.1208799109](https://doi.org/10.1073/pnas.1208799109)
- Sharp RV (1982a) Tectonic setting of the Imperial Valley Region, in the Imperial Valley earthquake of October 15, 1979. *US Geol Surv Profess Paper* 1254:5–14
- Sharp VR (1982b) Comparison of 1979 surface faulting with earlier displacements in the Imperial Valley, in *The Imperial Valley earthquake of October 15, 1979*. *US Geol Surv Profess Paper* 1254:213–221
- Sharp VR, Lienkaemper JJ, Bonilla MG et al (1982) Surface faulting in the central Imperial Valley, in *The Imperial Valley earthquake of October 15, 1979*. *US Geol Surv Profess Paper* 1254:119–143
- Steady S, Marsan D, Nalbant SS, McCloskey J (2004) Sensitivity of static stress calculations to the earthquake slip distribution. *J Geophys Res* 109:B04303. doi:[10.1029/2002JB002365](https://doi.org/10.1029/2002JB002365)
- Steady S, Nalbant SS, McCloskey J, Nostro C, Scotti O, Baumont D (2005) Onto what planes should Coulomb stress perturbations be resolved? *J Geophys Res* 110:15. doi:[10.1029/2004JB003356](https://doi.org/10.1029/2004JB003356)
- Stein RS (1999) The role of stress transfer in earthquake occurrence. *Nature* 402:605–609
- Stein RS (2003) Earthquake conversations. *Sci Am* 288(1):72–79
- Stein RS, Barka AA, Dieterich JH (1997) Progressive failure of North Anatolian Fault since 1939 by earthquake stress triggering. *Geophys J Int* 128:594–604
- Suarez-Vidal F, Mendoza-Borunda R, Nafarrete-Zamarripa LM, Ramirez J, Glowacka E (2008) Shape and dimensions of the Cerro Prieto pull-apart basin, Mexicali, Baja California, Mexico, based on the regional seismic record and surface structures. *Int Geol Rev* 50:636–649. doi:[10.2747/0020-6814.50.7.636](https://doi.org/10.2747/0020-6814.50.7.636)
- Sudhaus H, Jonsson S (2011) Source model for the 1997 Zirkuh earthquake (MW = 7.2) in Iran derived from JERS and ERS InSAR observations. *Geophys J Int* 185:676–692. doi:[10.1111/j.1365-246X.2011.04973.x](https://doi.org/10.1111/j.1365-246X.2011.04973.x)
- Talebian M, Jackson J (2002) Offset on the Main Recent fault of NW Iran and implications for the late Cenozoic tectonics of the Arabia-Eurasia collision zone. *Geophys J Int* 150:422–439
- Tan O (2004) Kafkasya, Doğu Anadolu ve Kuzeybatı İran Depremlerinin Kaynak Mekanizması Özellikleri ve Yırtılma Süreçleri. Dissertation, İstanbul Teknik Üniversitesi
- Toda S, Stein R (2003) Toggling of seismicity by the 1997 Kagoshima earthquake couplet: a demonstration of time-dependent stress transfer. *J Geophys Res* 108(B12):2567. doi:[10.1029/2003JB002527](https://doi.org/10.1029/2003JB002527)
- Toda S, Stein R, Richards-Dinger K, Bozkurt S (2005) Forecasting the evolution of seismicity in southern California: animations built on earthquake stress transfer. *J. Geophys. Res* 110:16. doi:[10.1029/2004JB003415](https://doi.org/10.1029/2004JB003415)
- Toda S, Stein RS, Beroza GC, Marsan D (2012) Aftershocks halted by static stress shadows. *Nat Geosci*. doi:[10.1038/NNGEO1465](https://doi.org/10.1038/NNGEO1465)
- USGS United States Geological Survey. <http://earthquake.usgs.gov/earthquakes/search/>. Accessed 10 Jan 2015
- Utkucu M (2013) 23 October 2011 Van, Eastern Anatolia, earthquake (Mw 7.1) and seismotectonics of Lake Van area. *J Seismol* 17:783–805. doi:[10.1007/s10950-012-9354-z](https://doi.org/10.1007/s10950-012-9354-z)
- Utkucu M, Pınar A, Alptekin Ö (2003) Uzak alan P dalga Şekillerinin sonlu-fay ters çözümünden 22 Mayıs 1971 Bingöl depremi kırılma sürecinin incelenmesi. *Yerbilimleri* 28:65–79
- Utkucu M, Durmus H, Yaşın H et al (2013) Coulomb static stress changes before and after the 23 October 2011 Van, eastern Turkey, earthquake (Mw = 7.1): implications for the earthquake hazard mitigation. *Nat Hazards Earth Syst Sci* 13:1–14. doi:[10.5194/nhess-13-1-2013](https://doi.org/10.5194/nhess-13-1-2013)
- Vernant P, Nilfouroushan F, Hatzfeld D et al (2004) Present-day crustal deformation and plate kinematics in Middle East constrained by GPS measurements in Iran and northern Oman. *Geophys J Int* 157:381–398. doi:[10.1111/j.1365-246X.2004.02222](https://doi.org/10.1111/j.1365-246X.2004.02222)
- Walker R, Jackson J, Baker C (2004) Active faulting and seismicity of the Dasht-e-Bayaz region, eastern Iran. *Geophys J Int* 157:265–282. doi:[10.1111/j.1365-2966.2004.02179.x](https://doi.org/10.1111/j.1365-2966.2004.02179.x)
- Walker RT, Bergman EA, Szeliga W, Fielding EJ (2011) Insights into the 1968–1997 Dasht-e-Bayaz and Zirkuh earthquake sequences, eastern Iran, from calibrated relocations, InSAR and high-resolution satellite imagery. *Geophys J Int*. doi:[10.1111/j.1365-246X.2011.05213.x](https://doi.org/10.1111/j.1365-246X.2011.05213.x)
- Wells DL, Coppersmith KJ (1994) New empirical relationships among magnitude, rupture length, rupture width, rupture area, and surface displacement. *Bull Seism Soc Am* 84(4):974–1002
- Zarifi Z, Nilfouroushan F, Raeesi M (2013) Crustal stress map of Iran: insight from seismic and geodetic computations. *Pure Appl Geophys* 171:1219–1236. doi:[10.1007/s00024-013-0711-9](https://doi.org/10.1007/s00024-013-0711-9)